

Characterizing dynamical phase transitions in a spinor Bose-Einstein condensate via quantum and semiclassical analyses

Zhen-Xia Niu

Department of Physics, Zhejiang Normal University, Jinhua 321004, China

Qian Wang

Department of Physics, Zhejiang Normal University, Jinhua 321004, China, and

*CAMTP-Center for Applied Mathematics and Theoretical Physics,
University of Maribor, Mladinska 3, SI-2000 Maribor, Slovenia*

(Dated: October 25, 2023)

Phase transitions in nonequilibrium dynamics of many body quantum systems, the so-called dynamical phases transition (DPTs), play an important role for understanding various dynamical phenomena observed in different branches of physics. In general, there have two types of DPTs, the first one refers to the phase transition that is characterized by distinct evolution behaviors of a physical observable, while the second one is marked by the nonanalyticities in the rate function of the initial state survival probability. Here, we focus on such DPTs from both quantum and semiclassical perspectives in a spinor Bose-Einstein condensate (BEC), an ideal platform to investigate nonequilibrium dynamics. By using the sudden quench process, we demonstrate that the system exhibits both types of DPTs present as the control parameter quenches through the critical one, referring to as the critical quench. We show analytically how to determine the critical quenches by means of the semiclassical approach and carry out a detailed examination on both semiclassical and quantum signatures of two types of DPTs. Moreover, we further reveal that the occurrence of DPTs is closely connected to the separatrix in the underlying classical system. Our findings provide more insights into the properties of DPTs and verify the usefulness of semiclassical analysis for understanding DPTs in quantum systems with well-defined semiclassical limit.

I. INTRODUCTION

The endeavor to reveal and understand exotic nonequilibrium phases of many body quantum systems has triggered a wide range of investigations of the dynamical phase transitions (DPTs). As an extension of the concept of equilibrium phase transition, DPTs refers the critical phenomena that happen in nonequilibrium dynamics of many body quantum systems [1–6]. The existence of DPTs has been verified in a variety of systems, such as the Hubbard model [2, 7–9], the Dicke [10] and Rabi models [11], different spin systems [12–21], as well as Floquet systems [22, 23], to name a few. Moreover, DPTs have also been observed in different experimental platforms involving trapped ions and cold atoms [24–28].

A typical scenario for exploring of DPTs in an isolated system consists of the following steps. First, the system is prepared in an initial state, usually the ground state, at a certain value of a control parameter. Then, the magnitude of the control parameter is suddenly changed from its initial value to a final value. Depending on the quench strength, the resulting dynamics may exhibit two different kinds of critical behaviors, dubbed as DPTs-I and DPTs-II, respectively. The first kind DPTs, denoted by DPTs-I, is signified by the changing of dynamics of a certain observable as the quench strength passes through the critical value [1–3, 10, 11, 29–35]. This leads to the using of long time average of such observable as the dynamical order parameter to define and distinguish different phases of DPTs-I, analogy to the equilibrium phase transitions.

Apart from DPTs-I, the dynamical critical behavior can also appear in the evolution of the initial state survival probability rate function, resulting in the concept of the second kind of DPTs [4, 5], referred to as DPTs-II. The definition of DPTs-II is based on the mathematical equivalence between the amplitude of the initial state survival probability and the boundary partition function. As a consequence, the nonanalytical behavior in the rate function at particular times is resembled to the singular behavior in the free energy at a critical temperature. Hence, a DPT-II is characterized by nonanalyticities in the rate function at particular instants of times, called the critical times. It is known that the occurrence of DPTs-II are independent of the equilibrium phase transitions [13, 36–39], and shows a strong dependence on the initial condition [18, 29, 40]. The connections between DPTs-I and DPTs-II have been discussed in several works [13, 33, 34, 40–43], however, a general relationship between them remains an open question.

In this work, we perform a detailed analysis of the properties of DPTs-I and DPTs-II in a spinor Bose-Einstein condensate (BEC) [44, 45] from both quantum and semiclassical perspectives. As a highly controllable platform, the spinor BECs have been extensively used, both theoretically and experimentally, to explore various nonequilibrium phenomena, such as the critical dynamics across the critical point of quantum phase transitions [46–54] and topological defects [55–57]. Here, by using aforementioned standard protocol in the studies of DPTs to a ferromagnetic spin-1 BEC, we focus on the critical behaviors in the evolution of a certain observable, as well as in the initial state survival probability rate function. We show that both kinds of DPTs are presented in the system as long as the sudden quench strength passes through the critical value. To uncover the triggering mechanism of DPTs, we analyze semiclassical limit of the system and discuss the correspondence between the quantum and semiclassical critical signatures of DPTs. We further demonstrate that both kinds of DPTs are closely linked to the separatrix in the underlying classical system. Hence, our results lead to a better understanding of the properties of DPTs and also verify the usefulness of the semiclassical analysis for studying DPTs in quantum systems with well-defined semiclassical limit. It is worth noting that the existence of DPT-I in antiferromagnetic spin-1 BEC has been explored from different aspects [28, 58–60]. However, in this work, we are interested in both kinds of DPTs in ferromagnetic spin-1 BEC and show how to understand them from the semiclassical viewpoint.

In the following, after introducing basic features of the spin-1 BEC and reviewing its semiclassical limit in Sec. II, we report our main results in Sec. III. Specifically, we first present our employed quench protocol and explain how to obtain the critical quench strength using the semiclassical analysis. Then, in Sec. IIIA, we provide a detailed investigation of the different signatures of DPT-I. We report our findings on DPT-II in Sec. IIIB and unveil the link between DPT-I and DPT-II. Finally, we conclude in Sec. IV with several remarks.

II. SPIN-1 SPINOR BOSE CONDENSATE

The spinor Bose-Einstein condensates (BECs) provide an excellent platform to explore a variety of interesting phenomena in condensate systems. In this work, we focus on a spinor BEC consisting of N spin-1 bose, such as ^{78}Rb or ^{23}Na atoms [44, 45, 61, 62], in an optical trap. Under the single-mode approximation, which assumes that all spin states have a same spatial wave function [63, 64], the system can be well described by the following Hamiltonian (setting $\hbar = 1$) [49, 65, 66]

$$\frac{H}{|c|} = \frac{\text{sign}(c)}{N} \left[(a_1^\dagger a_{-1}^\dagger a_0^2 + a_0^{\dagger 2} a_1 a_{-1}) + N_0(N_{+1} + N_{-1}) \right] + \xi(N_{-1} + N_{+1}). \quad (1)$$

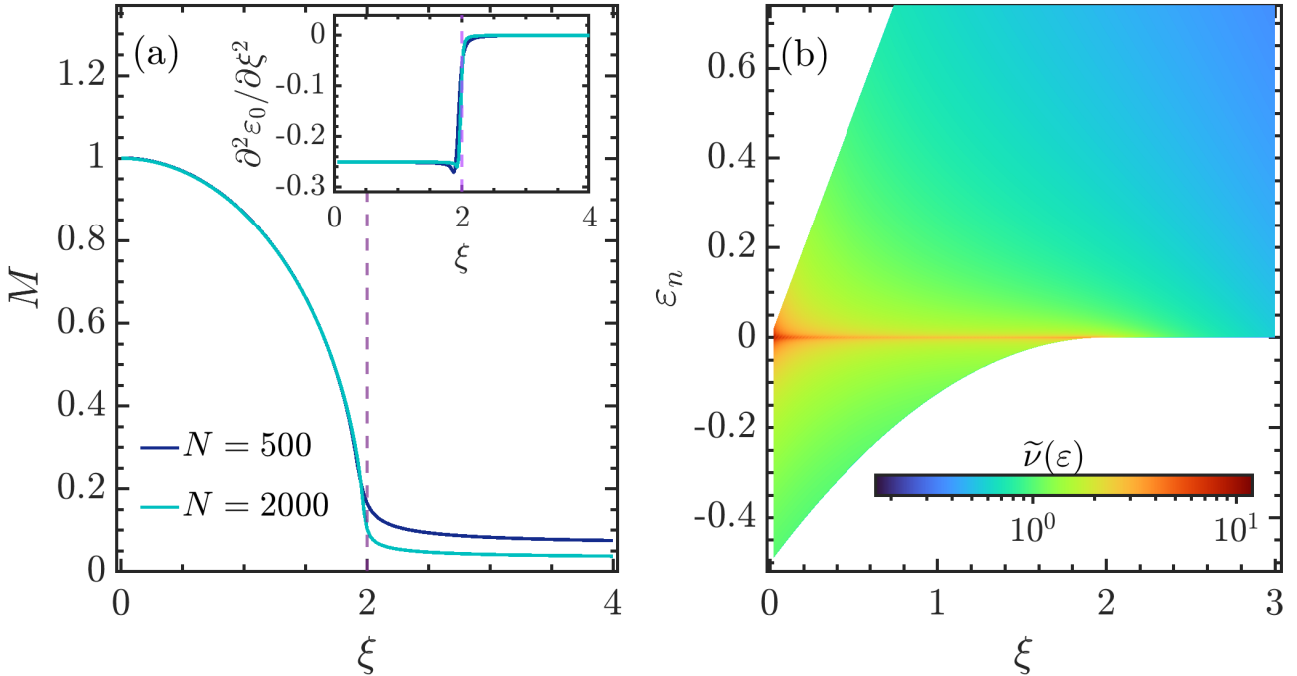


FIG. 1. (a) Order parameter M in (2) as a function of ξ for different system sizes. Inset: $\partial^2 \varepsilon_0 / \partial \xi^2$ as a function of ξ for same system sizes as in main panel. Here, $\varepsilon_0 = E_0/N$ with E_0 denotes the ground state energy. The vertical dashed lines in main panel and inset mark the critical value $\xi_c = 2$. (b) Rescaled density of states $\tilde{\nu}(\varepsilon) = (1/N) \sum_n \delta(\varepsilon - \varepsilon_n)$ as a function of ξ and rescaled eigenenergy $\varepsilon_n = E_n/N$ for a system with $N = 10000$. Here, the numerical result of $\tilde{\nu}(\varepsilon)$ is obtained from Eq. (9). All quantities are dimensionless.

Here, a_m and a_m^\dagger are the bosonic annihilation and creation operators of state $m = 0, \pm 1$, $N_m = a_m^\dagger a_m$ is the number operator and satisfies $\sum_m N_m = N$, c denotes the spin-dependent interaction strength with $c > 0$ ($c < 0$) for the antiferromagnetic (ferromagnetic) atoms, and $\xi \equiv q/|c|$ is the rescaled quadratic Zeeman shift, which can vary between positive and negative values via the microwave dressing [67, 68].

The Hamiltonian (1) conserves the total magnetization, $M = N_{+1} - N_{-1}$, and parity, $(-1)^{N_0}$. Hence, we restrict our study in the subspace of $M = 0$ with even parity, indicating that the Hilbert space has dimension $\mathcal{D}_H = N/2 + 1$ for even N . Moreover, we focus on the ferromagnetic condensate with $c < 0$ and positive quadratic Zeeman shift $\xi \geq 0$ in this work.

It is known that the ground state of Hamiltonian (1) undergoes a transition from the broken-axisymmetry (BA) phase to the polar phase as ξ passes through the critical point $\xi_c = 2$ [45, 49, 55, 68–70]. This is signified by the behavior of the order parameter, defined as [46–49]

$$M = \frac{\sqrt{\langle F_x^2 + F_y^2 \rangle}}{N}, \quad (2)$$

where $F_x = (F_+ + F_-)/2$, $F_y = (F_+ - F_-)/(2i)$ with $F_+ = \sqrt{2}(a_1^\dagger a_0 + a_0^\dagger a_{-1})$ and $F_- = F_+^\dagger$. The evolution of M as a function of ξ for different system sizes is shown in Fig. 1(a). As an order parameter of the ground state quantum phase transition, M is known for exhibiting a crossover from $M \neq 0$ in BA phase to $M = 0$ in polar phase as we straddle the critical point. Further evidence of the quantum phase transition at $\xi_c = 2$ is provided by the inset of Fig. 1(a), where we plot the second derivative of the rescaled ground state energy, $\varepsilon_0 = E_0/N$, as a function of ξ . An obvious sudden jump, which becomes more sharper with increasing N , around $\xi \approx 2$ clearly marks the second order phase transition at $\xi_c = 2$.

Apart from the ground state phase transition, the Hamiltonian (1) also exhibits an excited state quantum phase transition (ESQPT) in the BA phase [58, 71–73]. ESQPTs have been verified in a wide variety of many body quantum systems and show various impacts on both static and dynamical properties of systems, see Ref. [74] and references therein for a thoroughly review on different aspects of ESQPTs. First introduced as a generalization of ground state quantum phase transition, ESQPTs are characterized by the singularity in the density of states (DOS) at the critical energy [75]. For our studied spinor BEC, this is confirmed in Fig. 1(b), where we plot how the rescaled DOS,

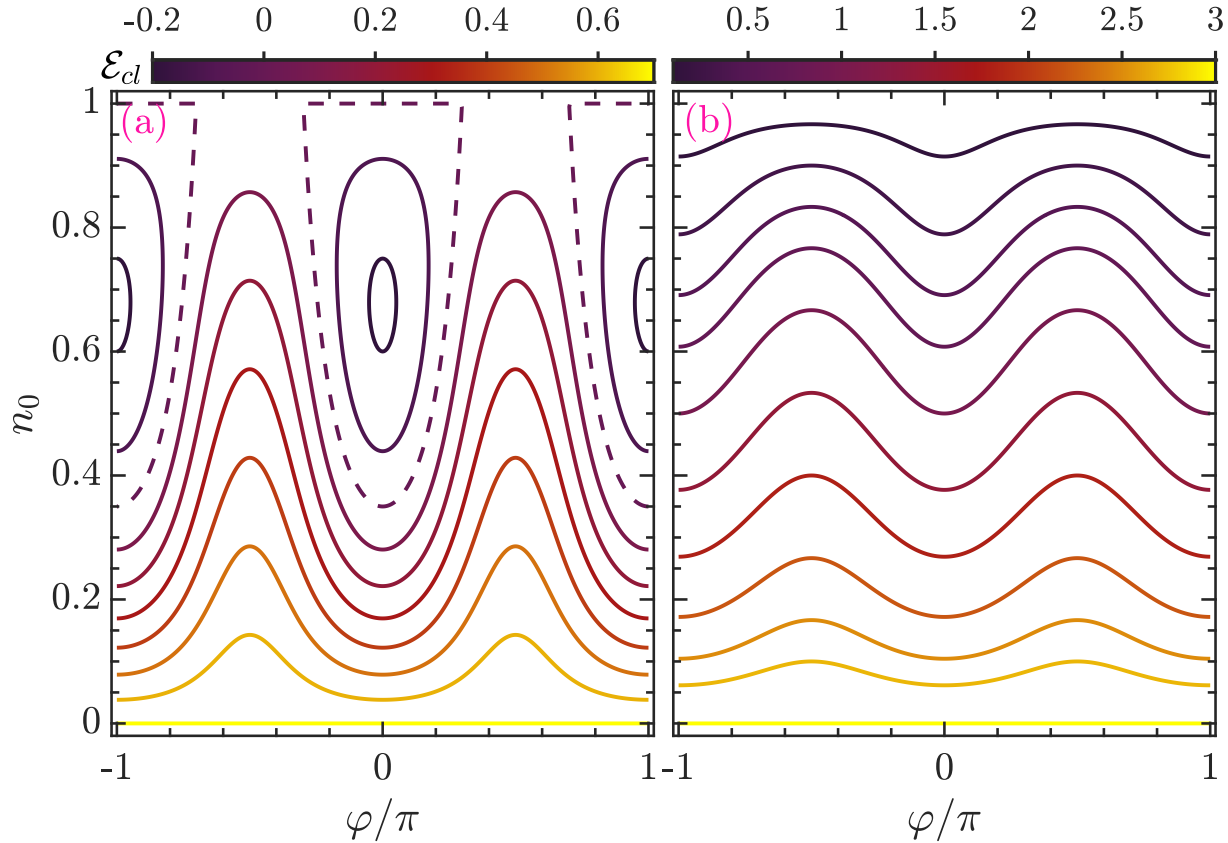


FIG. 2. Contour plot in the phase space of the classical Hamiltonian (5) for (a) $\xi = 1$ and (b) $\xi = 3$. The energy for each contour is indicated by the color bar. The dashed line in panel (a) marks the separatrix determined by $\mathcal{E}_{cl} = 0$. Panel (a) illustrates that the classical system has two degenerate minima and exhibits a separatrix in its dynamics. Panel (b) shows a connected phase space with minima is unique for the case of $\xi > \xi_c$. All quantities are dimensionless.

$\tilde{\nu}(\varepsilon) = (1/N) \sum_n \delta(\varepsilon - \varepsilon_n)$, varies as a function of ξ and rescaled energy $\varepsilon_n = E_n/N$. One see an obvious peak around $\varepsilon = 0$ in the behavior of $\tilde{\nu}(\varepsilon)$ as long as $\xi < \xi_c = 2$. The peak observed in $\tilde{\nu}(\varepsilon)$ serves as a finite size precursors of ESQPT and turns into the logarithmic divergence, $\tilde{\nu}(\varepsilon) \propto -\ln |\varepsilon - \varepsilon_c|$ with $\varepsilon_c = 0$, in the thermodynamic limit $N \rightarrow \infty$ [71, 75, 76].

Semiclassical limit

More insights into the properties of the system and associated phase transitions can be gained from the semiclassical analysis in the limit $N \rightarrow \infty$. To this end, we calculate the semiclassical counterpart of the Hamiltonian (1) by using the coherent states, defined as [58, 71, 77–79]

$$|\alpha\rangle = \frac{1}{\sqrt{N!}} \left(\sum_m \alpha_m a_m^\dagger \right)^N |0\rangle, \quad (3)$$

where $|0\rangle$ is the bosonic vacuum state, so that $a_m|0\rangle = 0$. Here, $\alpha_m = \sqrt{n_m} e^{i\phi_m}$ with $\phi_m \in [-\pi, \pi]$, $n_m \in [0, 1]$ and satisfies $\sum_m n_m = 1$. For our considered case with $N_{-1} = N_1$, the coherent state in Eq. (3) can be explicitly expressed as

$$|\alpha\rangle = \sum_{N_0=0}^N \binom{N}{N_0}^{1/2} (n_0)^{\frac{N_0}{2}} (1 - n_0)^{\frac{N - N_0}{2}} e^{-iN_0\varphi} |N, N_0\rangle, \quad (4)$$

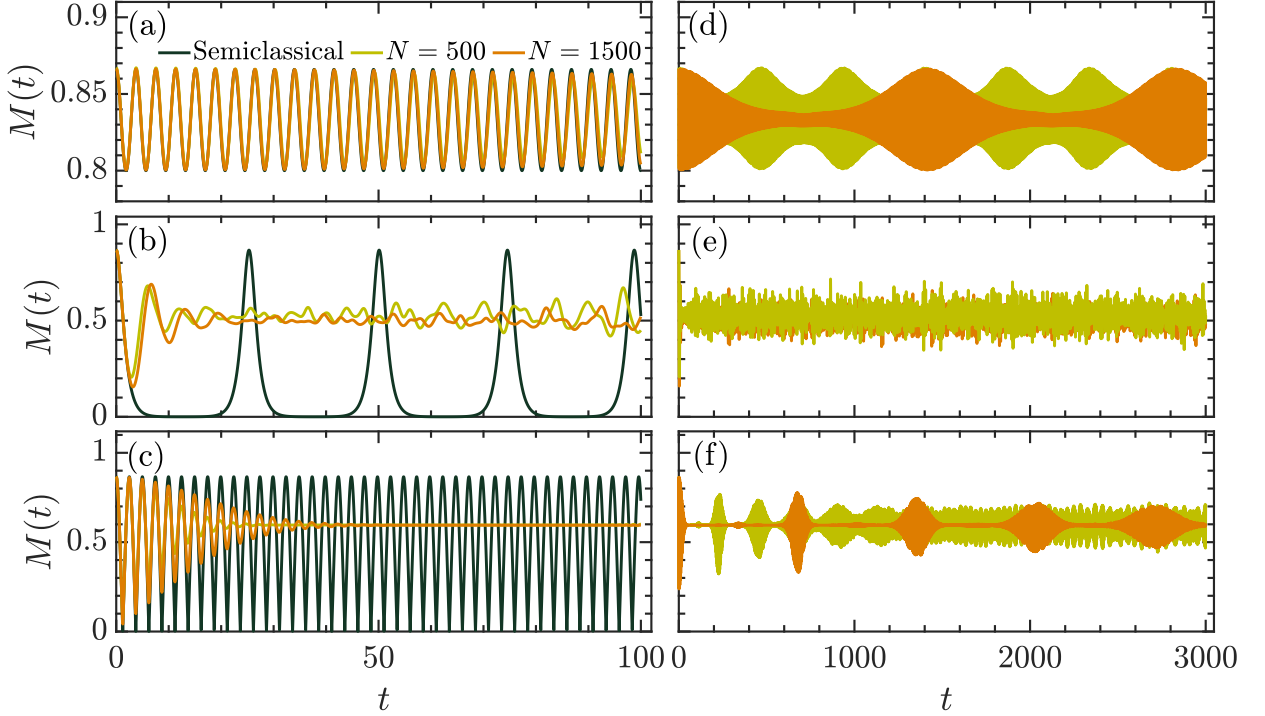


FIG. 3. Dynamics of the observable $M(t)$ (2) for different system sizes with [(a)(d)] $\delta\xi = 0.1$, [(b)(e)] $\delta\xi = 0.5$, and [(c)(f)] $\delta\xi = 1$. The color code in panel (a) is followed in all panels. In panels (a)-(c), dark green lines denote the semiclassical results. The initial state is the ground state of the system (1) with $\xi = \xi_i = 1$ and the critical quench strength is $\delta\xi_c = 0.5$ [see Eq. (14)]. The axes in all figures are dimensionless.

with $N_{-1} = N_1 = (N - N_0)/2$ and $|N, N_0\rangle$ are the Fock states. The classical limit of the model is given by the expectation value of H in Eq. (1) with respect to the coherent state in the classical limit $N \rightarrow \infty$. By employing the relation $\langle \alpha | a_m^\dagger a_m | \alpha \rangle = N \alpha_m^* \alpha_m$ [71, 79], one can easily find that the classical Hamiltonian with $N_1 = N_{-1}$ ($n_{-1} = n_1$) reads [71, 77]

$$\mathcal{H}_{cl} = \frac{1}{|c|} \lim_{N \rightarrow \infty} \frac{\langle \alpha | H | \alpha \rangle}{N} = \xi(1 - n_0) - 2n_0(1 - n_0) \cos^2 \varphi, \quad (5)$$

where $\varphi = \phi_0 - (\phi_1 + \phi_{-1})/2$ with $\phi_1 = \phi_{-1}$ is the relative phase. The classical equations of motion are

$$\begin{aligned} \dot{\varphi} &= \frac{\partial \mathcal{H}_{cl}}{\partial n_0} = -2(1 - 2n_0) \cos^2 \varphi - \xi, \\ \dot{n}_0 &= -\frac{\partial \mathcal{H}_{cl}}{\partial \varphi} = -2n_0(1 - n_0) \sin(2\varphi), \end{aligned} \quad (6)$$

associated with constrained condition $d(\phi_1 - \phi_{-1})/dt = 0$.

The fixed points of the classical system are the values $(\varphi_s, n_{0,s})$ that lead to $\dot{\varphi} = \dot{n}_0 = 0$. We first note that two fixed points $n_{0,s} = 0, 1$ are independent of ξ and φ values. The associated classical energy of them are given by $\mathcal{E}_{cl} = \xi$ and 0, respectively. However, the stability analysis tells us that the point $n_{0,s} = 0$ is an unstable fixed point for $\xi > 0$. On the contrary, the point $n_{0,s} = 1$ is stable for $\xi \geq \xi_c = 2$, while it becomes unstable when $\xi < \xi_c$. For the case of $\xi < \xi_c$, the stable fixed point of the system is provided by two degenerate points $(\cos \varphi_s, n_{0,s}) = [\pm 1, (2 + \xi)/4]$, corresponding to classical energy $\mathcal{E}_{cl} = -(2 - \xi)^2/8$. As a consequence, the rescaled ground state energy, which corresponds to the classical energy evaluated at the stable fixed points, can be written as

$$\varepsilon_0 = \mathcal{E}_{cl,s} = \begin{cases} -\frac{(2 - \xi)^2}{8} & \text{for } \xi < \xi_c, \\ 0 & \text{for } \xi \geq \xi_c. \end{cases} \quad (7)$$

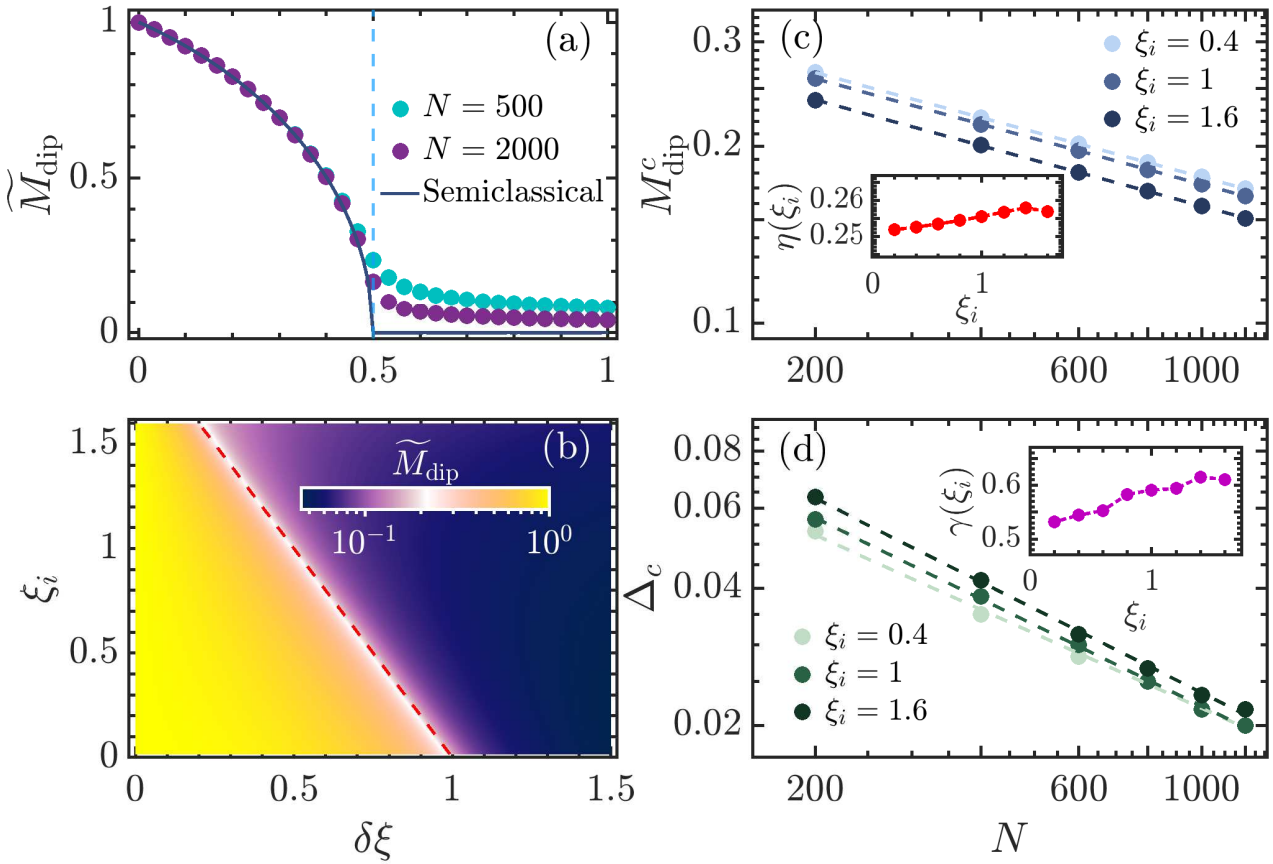


FIG. 4. (a) Rescaled M_{dip} , $\tilde{M}_{\text{dip}} = M_{\text{dip}}/M_{\text{dip}}^m$, as a function of $\delta\xi$ for different system sizes with $\xi_i = 1$, which yields $\delta\xi_c = 0.5$ [see Eq. (14)]. Here, M_{dip}^m is the maximal value of M_{dip} . The solid line denotes the semiclassical result and the vertical dashed line marks $\delta\xi_c = 0.5$. (b) \tilde{M}_{dip} as a function of $\delta\xi$ and ξ_i with $N = 1000$. The red dashed line marks the analytical critical line in (14). (c) Finite system size value of M_{dip} at $\delta\xi_c$, denoted by M_{dip}^c , as a function of N for several ξ_i values. The dashed lines represent the power law behavior of the form $M_{\text{dip}}^c \propto N^{-\eta(\xi_i)}$ with the dependence of the exponents $\eta(\xi_i)$ on ξ_i is shown in the inset. (d) Scaling of $\Delta_c = |\delta\xi_c(N) - \delta\xi_c|$ with system size N for several values of ξ_i . Here, $\delta\xi_c(N)$ is the precursor of the critical point and identified as the location of the minimal value of $\partial M_{\text{dip}}/\partial(\delta\xi)$. The dashed lines are the power law fitting, $\Delta_c \propto N^{-\gamma(\xi_i)}$. The inset plots how $\gamma(\xi_i)$ varies as a function of ξ_i . All quantities are dimensionless.

Clearly, the second derivative of ε_0 with respect to ξ undergoes a jump at $\xi_c = 2$, in agreement with the numerical results shown in the inset of Fig. 1(a). Moreover, in the classical limit with $N \rightarrow \infty$ the order parameter M reads [80]

$$\mathcal{M}_{\text{cl}} = \sqrt{4n_0(1 - n_0) \cos^2 \varphi} = \begin{cases} \frac{1}{2} \sqrt{4 - \xi^2} & \text{for } \xi < \xi_c, \\ 0, & \text{for } \xi \geq \xi_c. \end{cases} \quad (8)$$

It consists with the observed behaviors of M in the main panel of Fig. 1(a).

In Fig. 2, we show the energy contours in the phase space of the classical system (5) for different values of control parameter ξ . Each curve stands for the set of points (φ, n_0) that satisfies $\mathcal{H}_{\text{cl}}(\varphi, n_0) = \varepsilon$ with ε is a given energy. Note that the phase space for $\xi > \xi_c$ case is featureless and exhibits a global minimum at $n_0 = 1$, as seen in Fig. 2(b). However, as $n_0 = 1$ becomes a saddle point and two degenerate minima points appear for $\xi < \xi_c$, the phase space in this case exhibits a complex structure, as demonstrated in Fig. 2(a). The emergence of saddle point at $n_0 = 1$ with $\mathcal{E}_{\text{cl}} = 0$ implies the presence of separatrix in the underlying classical dynamics, as marked by the dashed lines in Fig. 2(a).

The coincidence between the critical energy of ESQPT and separatrix indicates that the occurrence of ESQPT can attribute to the existence of the saddle point in the corresponding classical system [75, 76]. This can be verified by the available phase space volume $\nu_{\text{cl}}(\varepsilon)$, which is the classical approximation of the quantum density of states [81]

and for our considered system is defined as [71]

$$\nu_{cl}(\varepsilon) = \frac{1}{2\pi} \int dn_0 d\varphi \delta(\varepsilon - \mathcal{H}_{cl}). \quad (9)$$

Here, we have taken into account the condition $n_{-1} = n_1$. One can evaluate the above integral by using the properties of the Dirac delta function. The leading behavior of $\rho_{cl}(\varepsilon)$ around the ESQPT critical energy $\varepsilon_c = 0$ is given by [44, 77, 82]

$$\lim_{\varepsilon \rightarrow \varepsilon_c} \nu_{cl}(\varepsilon) = -\frac{\ln |\varepsilon - \varepsilon_c|}{2\pi\sqrt{\xi(2-\xi)}}. \quad (10)$$

This asymptotic behavior confirms the close connection between the ESQPT in quantum system and the saddle point in the underlying classical system.

Above discussion demonstrates the usefulness of semiclassical approach for studying the characterizations of phase transitions in quantum model and inspires us to investigate whether it can help us to get a better understanding of the signatures of dynamical phase transitions (DPTs). In the rest of this article, we perform a detailed exploration on the DPTs in spinor BEC and show how to understand the main characters of DPTs from the corresponded classical dynamics.

III. DYNAMICAL PHASE TRANSITIONS

The term DPTs refer two kinds of phase transitions, denoted by DPTs-I and DPTs-II, respectively. The first kind, DPTs-I, is identified by the non-equilibrium order parameter, which defines as a long-time average of a certain observable and undergoes an abrupt change at the critical point that divides different dynamical phases [2, 8–11, 30–35, 83]. Typically, DPTs-I are studied by means of a quantum quench, which is a sudden change of control parameters in the system and results in the non-equilibrium dynamics. It is closely related to prethermalization [84, 85] and has been observed in numerous experiments [3, 25–28].

Despite the second type, DPTs-II, also induced by the sudden quench process in isolated quantum systems, it is characterized by singularities in the Loschmidt echo rate function at critical times [4, 5], instead of the nonanalytical behaviors in the dynamical order parameter. It was originally defined in the one-dimensional Ising model and attracted a great deal of effort to study various aspects in a variety of quantum systems [16–24, 33–35, 86–88]. The DPTs are independent of the equilibrium phase transitions [2, 37], but a general relationship between two types of DPTs is still an open question [12–15, 32, 42].

In this work, we focus on both types of DPTs in the spin-1 spinor BEC. To this end, we consider the following quench process. The system is initially prepared in the ground state, $|\psi_0\rangle$, of the initial Hamiltonian H_i obtained by fixing $\xi = \xi_i < \xi_c$ in (1). Then, at $t = 0$, we suddenly change the value of ξ from its initial value ξ_i to a certain final value $\xi_f = \xi_i + \delta\xi$. Now, as the initial state is not the eigenstate of the final Hamiltonian $H_f = H(\xi_f)$ anymore, it starts to evolved. At time t , the density of state of the system is given by

$$\rho(t) = |\psi_t\rangle\langle\psi_t| = e^{-iH_f t}|\psi_0\rangle = \sum_{n,k} c_n^* c_k e^{-i(E_k^f - E_n^f)t} |E_k^f\rangle\langle E_n^f|, \quad (11)$$

where $|E_k^f\rangle$ is the k th eigenstate of H_f with energy E_k^f , so that $H_f|E_k^f\rangle = E_k^f|E_k^f\rangle$, and $c_k = \langle E_k^f | \psi_0 \rangle$ is the overlap between $|E_k^f\rangle$ and the initial state.

The sudden quench of the value of control parameter from ξ_i to ξ_f leads to the change of the initial state energy. The energy of the quenched initial state can be calculated using the classical approach with the result given by

$$\mathcal{E}_f(\xi_i, \delta\xi) = \frac{1}{N} \langle \psi_0 | H_f | \psi_0 \rangle = \mathcal{H}_{cl}^f|_{(\varphi_s, n_{0,s})}, \quad (12)$$

where \mathcal{H}_{cl}^f is the classical limit version of H_f and $(\varphi_s, n_{0,s})$ is the initial state corresponded fixed point. Then, by inserting $\varphi_s = \arccos(\pm 1)$ and $n_{0,s} = (\xi_i + 2)/4$ into above equation, it is straightforward to find that the explicit form of $\mathcal{E}_f(\xi_i, \delta\xi)$ can be expressed as

$$\mathcal{E}_f(\xi_i, \delta\xi) = \frac{2 - \xi_i}{8} [2\delta\xi - (2 - \xi_i)]. \quad (13)$$

Hence, the energy of the quenched system can be varied by tuning the quench strength $\delta\xi$. The existence of the separatrix for $\xi_i < 2$ in the classical dynamics implies that there has a critical quench strength $\delta\xi_c$, which takes

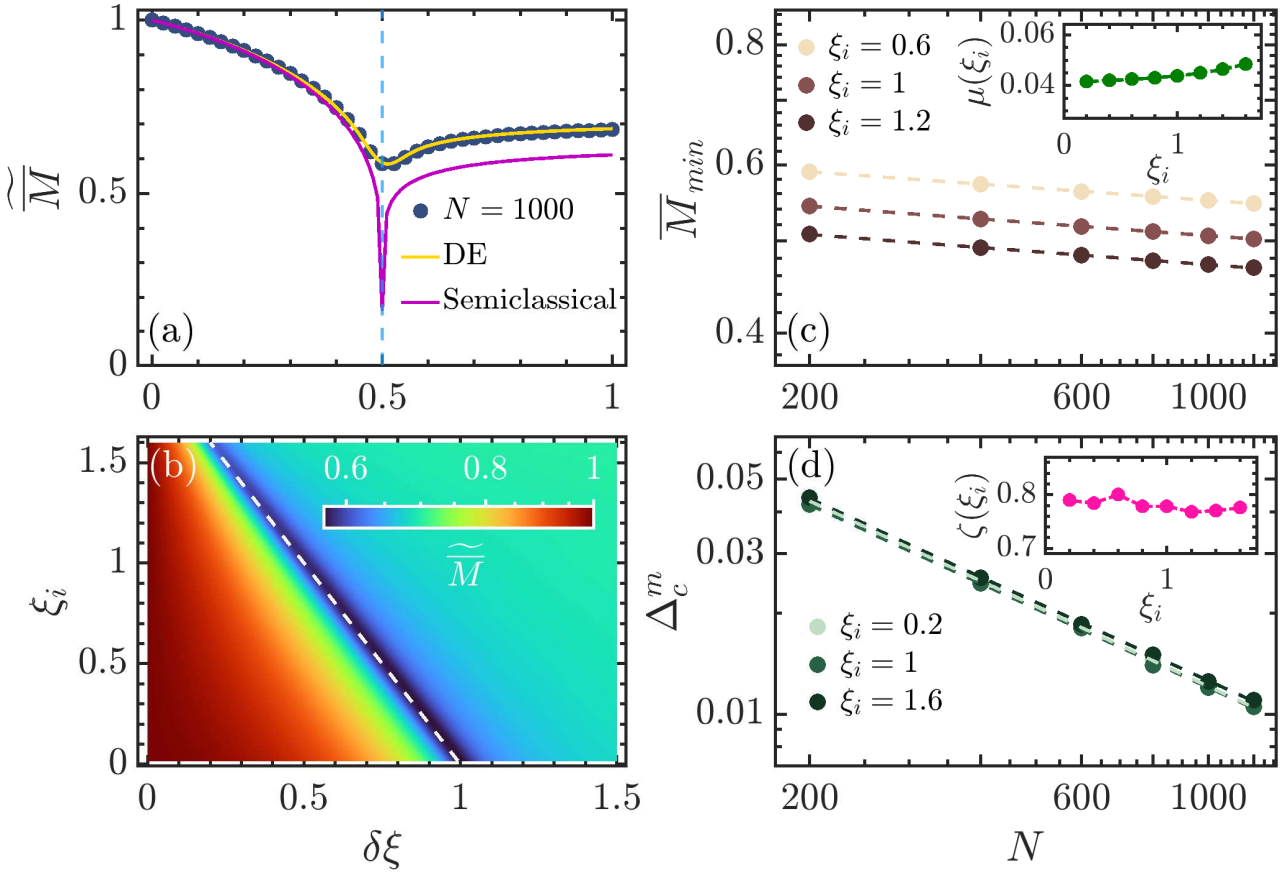


FIG. 5. (a) Rescaled long time average of $M(t)$ in (16), $\widetilde{M} = \overline{M}/\overline{M}_{max}$, as a function of $\delta\xi$ for $\xi_i = 1$, so that $\delta\xi_c = 0.5$ [see Eq. (14)], marked by vertical dashed line. Here, \overline{M}_{max} denotes the maximal value of \overline{M} . Full circles are the numerical results for $N = 1000$, obtained in the time interval $t \in [0, 1000]$. The yellow solid line is obtained using the diagonal ensemble average in (17), while the purple solid line represents the semiclassical result. (b) \widetilde{M} as a function of ξ_i and $\delta\xi$ with $N = 1000$. The white dashed line marks the analytical critical line in Eq. (14). (c) Minimal value of \overline{M} , denoted by \overline{M}_{min} , as a function of N for several ξ_i values. The dashed lines represent the power law scaling of the form $\overline{M}_{min} \propto N^{-\mu(\xi_i)}$ with the dependence of $\mu(\xi_i)$ on ξ_i is shown in the inset. (d) Scaling of $\Delta_c^m = |\delta\xi_c^m(N) - \delta\xi_c|$ with system size N for several values of ξ_i . Here, $\delta\xi_c^m(N)$ is the precursor of the critical point and it has been identified as the position of \overline{M}_{min} . The dashed lines are the power law fitting, $\Delta_c^m \propto N^{-\zeta(\xi_i)}$. The variation of $\zeta(\xi_i)$ with ξ_i is plotted in the inset. The axes in all figures are dimensionless.

the quenched system to the energy of the separatrix, which is given by $\mathcal{E}_{cl,sp} = 0$. For the energy below \mathcal{E}_s the classical phase space possesses two disjointed regions, while these regions are merged together for $\mathcal{E}_f(\xi_i, \delta\xi) > \mathcal{E}_{cl,sp}$, see Appendix A for further details. From the condition $\mathcal{E}_f(\xi_i, \delta\xi) = \mathcal{E}_{cl,sp} = 0$, one can easily find that the critical quench strength is given by

$$\delta\xi_c = 1 - \frac{\xi_i}{2}, \quad (14)$$

with $0 < \xi_i < 2$. In the following of this section, we investigate the consequences of the separatrix in nonequilibrium dynamics with the aim to explore various dynamical phases.

A. DPTs-I: dynamical order parameters

The first type of DPTs, DPTs-I, is signified by different evolution behavior of a physically relevant observable as the system control parameter varies. Here, we choose M in Eq. (2) as our studied observable. The discussion for the

case of other observable can be found in Appendix B. After quench, the time evolution of M reads

$$M(t) = \text{Tr}[\rho(t)M] = \sum_{n,k} c_n^* c_k e^{-i(E_k^f - E_n^f)t} M_{kn}, \quad (15)$$

where $M_{nk} = \langle E_k^f | M | E_n^f \rangle$. We also study the evolution of $\mathcal{M}_{cl}(t)$ in (8), which is the classical counterpart of $M(t)$ and is completely governed by the classical equations of motion Eq. (6). As the quantum dynamics approaches the classical one with increasing the system size N , the evolution of $M(t)$ should be well captured by $\mathcal{M}_{cl}(t)$ in the large N limit.

In Figs. 3(a)-3(c), we plot the time evolutions of $M(t)$ for several quenching strengths and system sizes with $\xi_i = 1$, which yields $\delta\xi_c = 0.5$ according to Eq. (14). The evolutions of $\mathcal{M}_{cl}(t)$ for each case are depicted with dark green lines. Overall, the behavior of $M(t)$ exhibits a strong dependence on the quenching strength. Specifically, for $\delta\xi < \delta\xi_c = 0.5$, as illustrated in Fig. 3(a), $M(t)$ undergoes a regular oscillation with small amplitude and follows the classical dynamics even for relatively small system size. This due to the fact that the quenched state for small quenching strengths remains within one of the two classical wells and oscillates around the initial fixed point with a same frequency as the classical counterpart. On the contrary, the evolution of $M(t)$ undergoes a remarkable change for the quenching strengths that above the critical value, such as $\delta\xi = 1$ case plotted in Fig. 3(c). For quenches with $\delta\xi > \delta\xi_c$, the quenched system has enough energy and the corresponded classical dynamics can explore both wells in the phase space. As a result, the evolution of $\mathcal{M}_{cl}(t)$ oscillates regularly with large amplitude. However, we see damping combined with dephasing in the quantum dynamics. Moreover, the deviation time between the quantum and classical dynamics is very short, even for large system size. The distinct difference in the evolutions of $M(t)$ and $\mathcal{M}_{cl}(t)$ suggests that quantum correlations have significant impacts on the quantum dynamics when $\delta\xi > \delta\xi_c$. The critical quench is demonstrated in Fig. 3(b), where the quenched system has energy coincides with the energy of separatrix. Classically, the evolution of the system will spend long time at the saddle point $\rho_{0,f} = 1$, leading to the low frequency of the oscillation of $\mathcal{M}_{cl}(t)$. A drastic deviation from the behavior of $\mathcal{M}_{cl}(t)$ in the evolution of $M(t)$ can be clearly identified in this critical case. The separatrix in the underlying classical system leads to a quite fast equilibration process in the quantum dynamics

The longer time evolution of the same state as in Figs. 3(a)-3(c) are shown in Figs. 3(d)-3(f). As seen in the short time behaviors, the evolution of $M(t)$ in the longer time scale still depends on whether the value of $\delta\xi$ is below, at, or above the critical value. Generally, for noncritical quenches, $M(t)$ oscillates around its steady state value and shows dynamical revivals at later times, as clearly seen from Figs. 3(d) and 3(f). The dynamical revival is an echo of the short time behaviors of a physical quantity and is a consequence of the discreteness in the spectrum of the system [89, 90]. The time for the first revival and the time interval between two succeeding revivals increase as the system size N increases. One can expect that the revival patterns will disappear and $M(t)$ behaves very noisy at very long times. This is already visible in Fig. 3(f) for $N = 500$ case. The situation for the critical quench in Fig. 3(e) shows a complete different scenario. There is no revival in quantum dynamics and $M(t)$ evolves with erratic fluctuations around its equilibrium value.

The results displayed in Fig. 3 neatly manifest the predominant signature of DPTs-I: a significant change in the dynamical behaviors of physical observables as the control parameter is varied. Further evidence of the occurrence of DPTs-I as the quenching strength passes through the critical value is provided by a close inspection on the first dip value of $M(t)$, defined as $M_{\text{dip}} = M(t = \tau_{\text{dip}})$ with τ_{dip} being the time when the first dip present. The short time behavior of $M(t)$ in Figs. 3(a)-3(c) shows that M_{dip} has a large value for $\delta\xi < \delta\xi_c$, while it approaches zero as soon as $\delta\xi > \delta\xi_c$. This allows us to take M_{dip} as an order parameter of DPT-I for the Hamiltonian (1).

Figure 4(a) plots M_{dip} as a function of $\delta\xi$ for several system sizes with $\xi_i = 1$. In the same figure, we also show the corresponded classical result which obtains from the first dip in the evolution of $\mathcal{M}_{cl}(t)$. One see that M_{dip} takes a nonzero value and decreases with increasing $\delta\xi$ before the critical point has been crossed, whereas it tends to vanish as long as the system passes through the critical point. The transition in M_{dip} is smooth for finite system sizes, rather than the abrupt change observed in the classical result. However, the crossover from $M_{\text{dip}} \neq 0$ to $M_{\text{dip}} = 0$ becomes sharper and tends towards the classical results as the system size increases. The dependence of M_{dip} as a function of $\delta\xi$ and ξ_i is depicted in Fig. 4(b). One can clearly see that the phase boundary determined by the dramatic change in the behavior of M_{dip} is in good agreement with the analytical result. We would like to point out that the abrupt change in the behavior of M_{dip} can also be recognized as a dynamical effect of separatrix in the classical counterpart. For $\delta\xi < \delta\xi_c$, the dynamics is restricted within one of two disconnected potential wells with $\rho_0 \neq 0$ and $\cos\varphi \neq 0$ for all t , resulting in positive $M(t)$. By contrast, the dynamics can explore two classical wells as long as $\delta\xi > \delta\xi_c$. This entails the zero value in $\cos\varphi$, leading to the presence of zero points in the evolution of $M(t)$.

Further signatures of the DPT-I are revealed by performing the scaling analysis. In Fig. 4(c), we show the scaling of the value of M_{dip} at $\delta\xi_c$, denoted by M_{dip}^c , with the system size N for several ξ_i values. The decay of M_{dip}^c with increasing N is well captured by a power law of the form $M_{\text{dip}}^c \propto N^{-\eta(\xi_i)}$ with $\eta(\xi_i) \approx 0.255$ almost independent of ξ_i ,

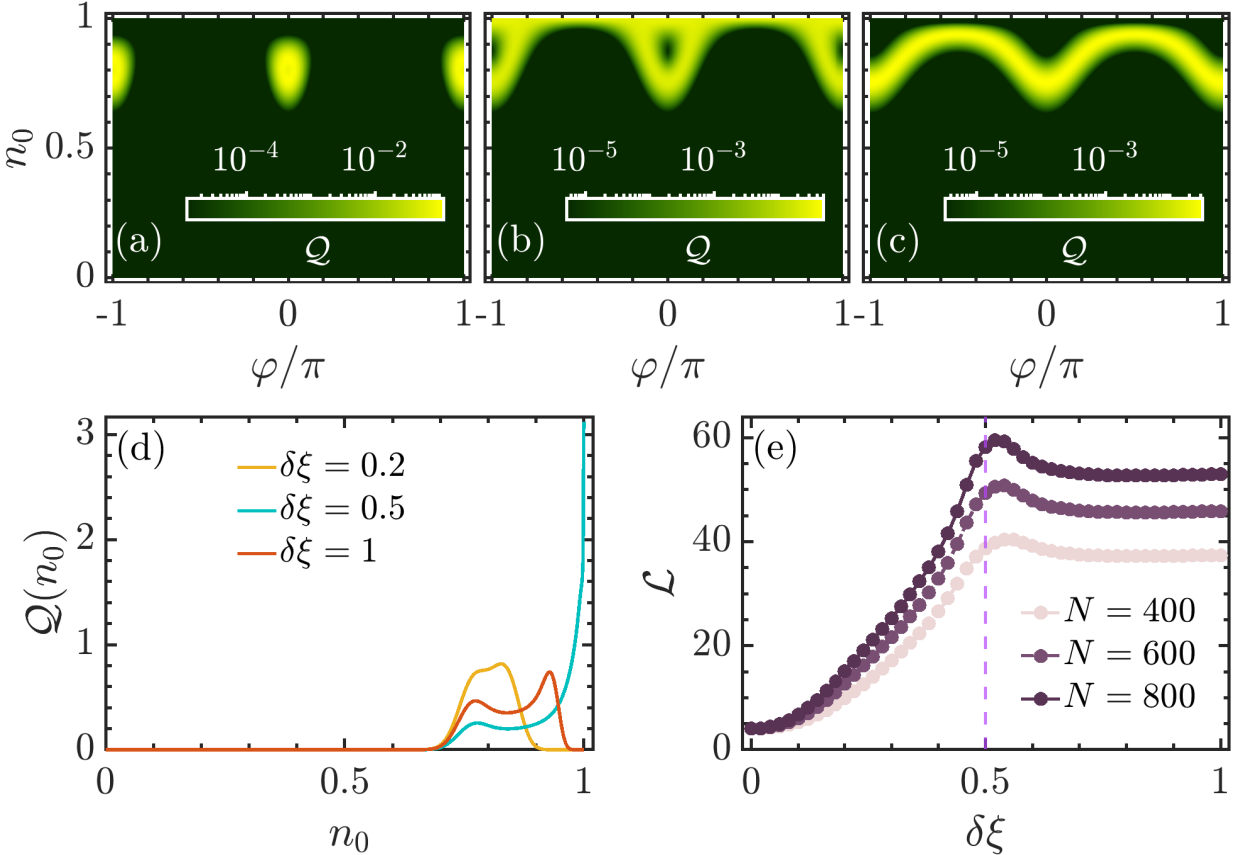


FIG. 6. Husimi function $Q(n_0, \varphi)$ for (a) $\delta\xi = 0.2$, (b) $\delta\xi = 0.5$, and (c) $\delta\xi = 1$ with system size $N = 600$. (d) Marginal distribution of the Husimi function, $Q(n_0)$ as a function of n_0 for several $\delta\xi$ values with $N = 600$. (e) Phase space localization measure \mathcal{L} as a function of $\delta\xi$ for several system sizes. Vertical dashed line marks the critical point, $\delta\xi_c$, of DPT-I. Other parameters: $\xi_i = 1$ and $\delta\xi_c = 0.5$ obtained from (14). All quantities are dimensionless.

as demonstrated in the inset in Fig. 4(c). More scaling properties in M_{dip} can be obtained by considering the finite- N precursor of the critical point $\delta\xi_c(N)$. To this end, we identify the location of the minimal value in $\partial M_{\text{dip}}/\partial(\delta\xi)$ as $\delta\xi_c(N)$. The difference between the numerical results and the analytical critical point $\delta\xi_c$ in (14), $\Delta_c = |\delta\xi_c(N) - \delta\xi_c|$, evolves as a function of N for several ξ_i values is plotted in Fig. 4(d). Again, we see the dependence of Δ_c on the system size is well fitted by the power law decay, $\Delta_c \propto N^{-\gamma(\xi_i)}$ with the decay exponent $\gamma(\xi_i)$ increases with increasing ξ_i , as seen in the inset of Fig. 4(c). These results confirm that the system undergoes the DPT-I in the classical limit.

Long time average of $M(t)$

The DPTs-I are also signified by the singular behaviors in the long time average of a certain physical observable. Now we focus on the properties of the long time average of $M(t)$, defined as

$$\overline{M} = \overline{\overline{M}(t)} = \lim_{T \rightarrow \infty} \frac{1}{T} \int_0^T M(t) dt. \quad (16)$$

Substituting $M(t)$ in (15) into above equation and note that there is no degeneracies in the spectrum, it is easy to find that \overline{M} can be recast as

$$\overline{M} = \sum_n |c_n|^2 M_{nn} = \text{Tr}[\overline{\rho} M], \quad (17)$$

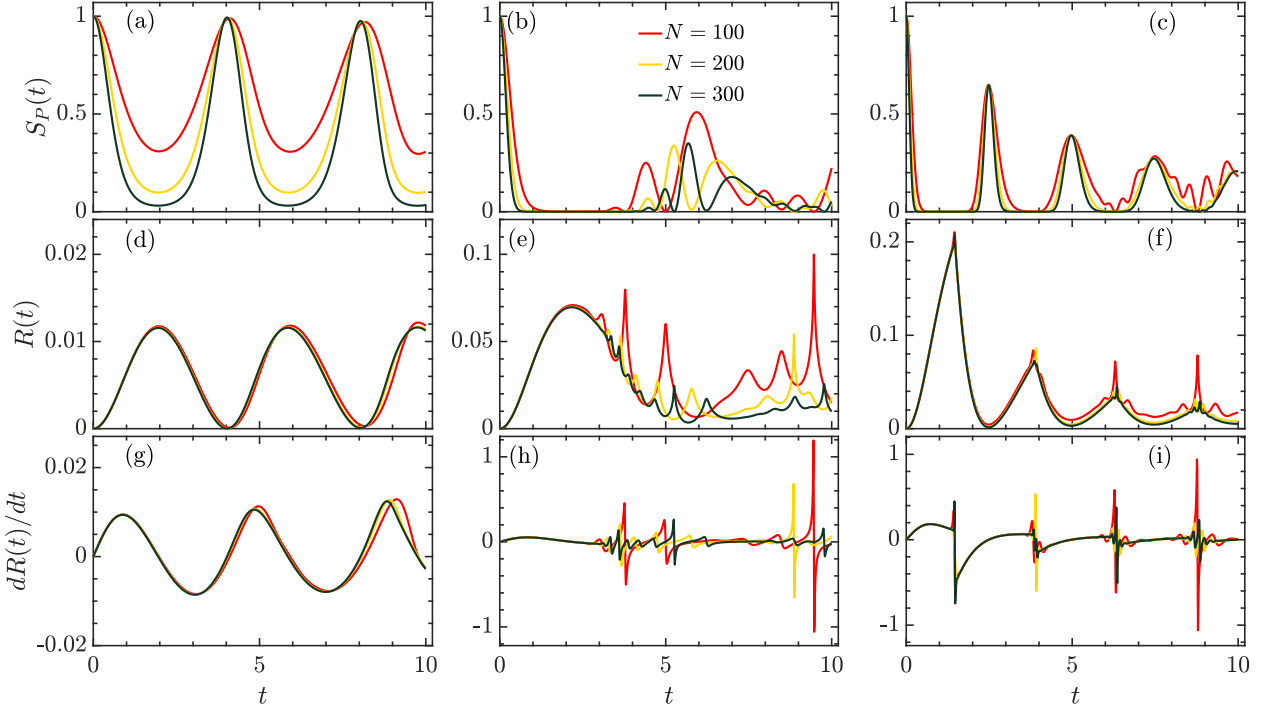


FIG. 7. Time evolution of the survival probability $S_P(t)$ for (a) $\delta\xi = 0.2$, (b) $\delta\xi = 0.5$, and (c) $\delta\xi = 1$, and for different system sizes [see the legend in panel (d)]. (d)-(f): Rate function $R(t)$ corresponding to $S_P(t)$ in panels (a)-(c), respectively. (g)-(i): Time derivatives $dR(t)/dt$ for $R(t)$ in panels (d)-(f). The legend in panel (b) is used in all panels. Other parameters: $\xi_i = 1$ and $\delta\xi_c = 0.5$ obtained from (14). The axes in all figures are dimensionless.

where

$$\bar{\rho} = \lim_{T \rightarrow \infty} \frac{1}{T} \int_0^T \rho(t) dt = \sum_n |c_n|^2 |E_n\rangle \langle E_n|, \quad (18)$$

is the long time averaged density of state. Notice that this result is in agreement with the diagonal ensemble (DE) [91, 92].

The calculation of \bar{M} has been conducted for several quenches, letting the evolution of the quenched system during $T = 1000$. The final long time averages for a system with $N = 1000$ and $\xi_i = 1$ are plotted as a function of $\delta\xi$ in Fig. 5(a). Moreover, the long time averages obtained from DE and classical approximation are also shown in the same figure. Irrespective of the method used, we see that the critical point is marked by an abrupt dip in the behavior of \bar{M} . Additionally, an excellent agreement between the numerical and the DE results is clearly visible. However, despite the classical result provides a good description of the quantum behavior in $\delta\xi < \delta\xi_c$ phase, it fails to follow the behavior of \bar{M} for $\delta\xi > \delta\xi_c$. This is due to the existence of significant quantum correlations in the evolution of $M(t)$, as has already been manifested in Fig. 3(c).

The dip exhibited by \bar{M} near the critical point implies that it can be taken as the precursor of the critical point of DPT-I. This can be appreciated in Fig. 5(b), where we depict how \bar{M} varies as a function of $\delta\xi$ and ξ_i . As can be seen, the critical line in (14) is perfectly reproduced by the dip in \bar{M} . To strengthen above statement, we analyze the scaling of the minimal \bar{M} value, \bar{M}_{min} . Figure 5(c) plots \bar{M}_{min} as a function of N for several ξ_i values. With increasing system size N , the decrease of \bar{M}_{min} is well described by the power law of the form $\bar{M}_{min} \propto N^{-\mu(\xi_i)}$ with $\mu(\xi_i) \approx 0.044$. An explicit dependence of $\mu(\xi_i)$ on ξ_i is shown in the inset of Fig. 5(c). Hence, the dip in \bar{M} becomes sharp as the system size is increased. Moreover, by defining the precursor of the critical point of DPT-I, $\delta\xi_c^m(N)$, as the position of \bar{M}_{min} , we further investigate how the deviation between $\delta\xi_c^m(N)$ and $\delta\xi_c$ in (14), $\Delta_c^m = |\delta\xi_c^m(N) - \delta\xi_c|$, evolves as a function of the system size. The results for different ξ_i values are demonstrated in Fig. 5(d). One can see that Δ_c^m exhibits an obvious power law decay $\Delta_c^m \propto N^{-\zeta(\xi_i)}$, regardless of the values of ξ_i . The decay exponent $\zeta(\xi_i)$ is approximately independent of ξ_i and given by $\zeta(\xi_i) \approx 0.7805$, as visualized in the inset of Fig. 5(d). This confirms that the emergence of DPT-I is characterized by the dip in the long time average of $M(t)$.

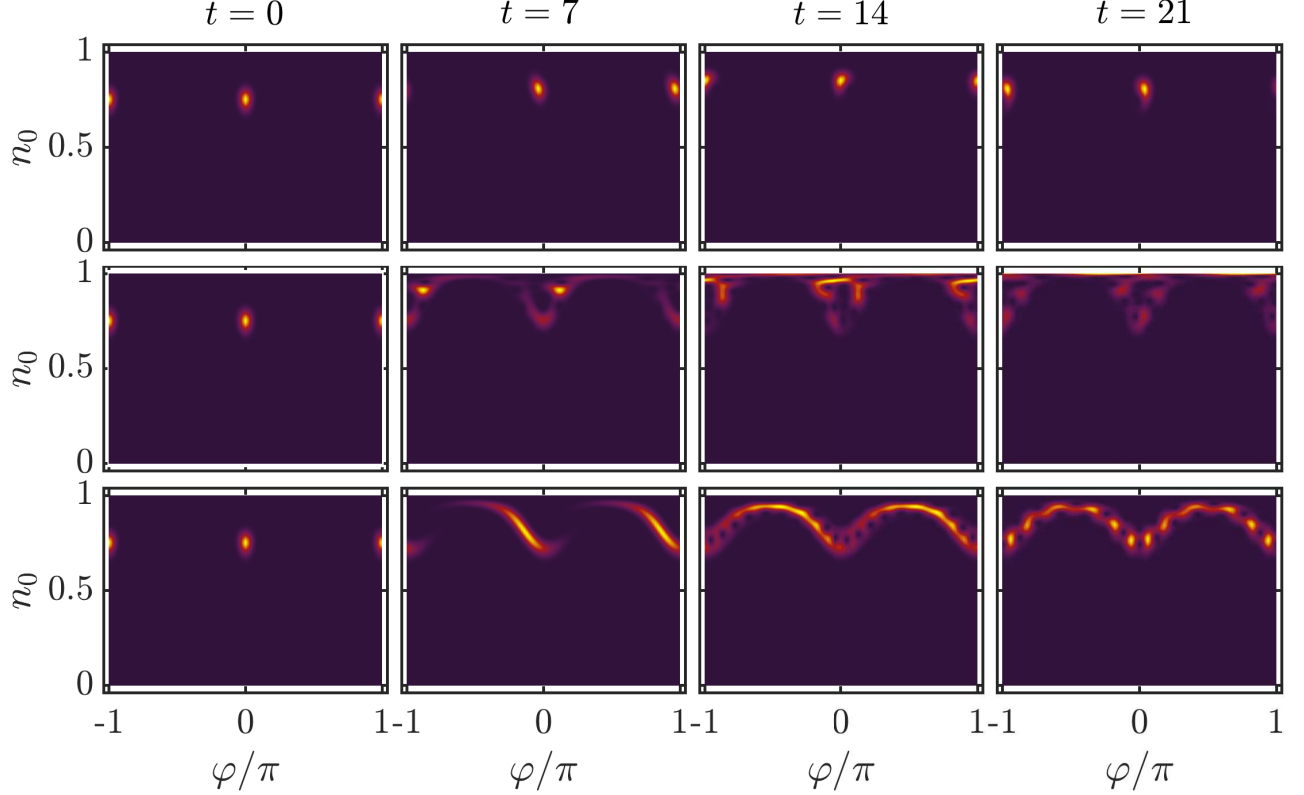


FIG. 8. Snapshots of the evolved Husimi function $\mathcal{Q}_t(n_0, \varphi)$ at different time steps with $\delta\xi = 0.2, 0.5$, and 1 (from top to bottom rows). Other parameters: $N = 300$ and $\xi_i = 1$ which yields $\delta\xi_c = 0.5$ [cf. Eq. (14)]. The axes in all figures are dimensionless.

The abrupt decrease exhibited by \overline{M} around the critical point is also a manifestation of the separatrix in the classical dynamics. Classically, since the separatrix associated with the saddle point, the initial state evolves into a rather delocalized state along the separatrix. Consequently, both classical and quantum evolutions of the order parameter are able to reach very small values, giving rise to a remarkable dip in \overline{M} near the critical point of DPT-I. To illustrate how the extension of the long time averaged state depends on the quenching strength, we consider the Husimi function [93]. The Husimi function is the Gaussian smooth of the well known Wigner function [94] and provides a useful tool for studying quantum-classical correspondence in various systems. In the classical limit, the Husimi function behaves as a classical probability distribution in phase space and evolves according to the Liouville equation [95, 96]. For the state $\overline{\rho}$, the Husimi function can be written as

$$\mathcal{Q}(n_0, \varphi) = \langle \alpha | \overline{\rho} | \alpha \rangle = \sum_n |c_n|^2 |\langle \alpha | E_n \rangle|^2, \quad (19)$$

where $|\alpha\rangle$ is the coherent states in (3) with $N_{-1} = N_1$. The normalization condition of $\mathcal{Q}(n_0, \varphi)$ is given by

$$\frac{N+1}{2\pi} \int dn_0 d\varphi \mathcal{Q}(n_0, \varphi) = 1. \quad (20)$$

Density plots of $\mathcal{Q}(n_0, \varphi)$ for several $\delta\xi$ values in a system with $N = 1000$ and $\xi_i = 1$ are shown in Figs. 6(a)-(c). The largest extension of $\overline{\rho}$ in the phase space for the critical quench $\delta\xi_c = 0.5$ is clearly visible. In particular, we see that the Husimi function for $\delta\xi_c = 0.5$ case shows an obvious distribution the line of $n_0 = 1$. This is more evidenced in the behavior of the marginal distribution of the Husimi function, defined as

$$\mathcal{Q}(n_0) = \sqrt{\frac{N+1}{2\pi}} \int d\varphi \mathcal{Q}(n_0, \varphi), \quad (21)$$

with normalization condition

$$\sqrt{\frac{N+1}{2\pi}} \int dn_0 \mathcal{Q}(n_0) = 1. \quad (22)$$

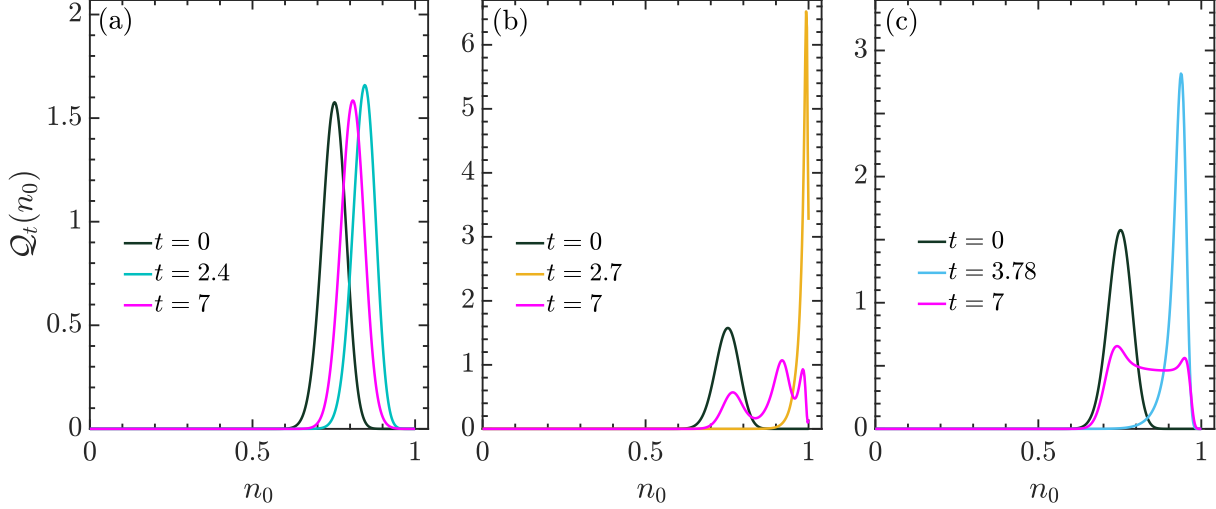


FIG. 9. Marginal distribution, $Q_t(n_0)$, of the time evolved Husimi function at different times for (a) $\delta\xi = 0.2$, (b) $\delta\xi = 0.5$, and (c) $\delta\xi = 1$. Other parameters: $N = 300$ and $\xi_i = 1$, so that $\delta\xi_c = 0.5$ [cf. Eq. (14)]. The axes in all figures are dimensionless.

It is the projection of the Husimi function in the n_0 -space. Figure 6(d) shows how $Q(n_0)$ varies as a function of n_0 for the same values of $\delta\xi$ as in Figs. 6(a)-(c). The condensation of the Husimi function along $n_0 = 1$ observed in Fig. 6(b) is unambiguously confirmed by the highest peak in $Q(n_0)$ at $n_0 = 1$ for $\delta\xi = \delta\xi_c = 0.5$ case.

The degree of extension of the state $\bar{\rho}$ can be quantified by the phase space localization measure, defined as

$$\mathcal{L} = \left[\frac{N+1}{2\pi} \int dn_0 d\varphi Q^2(n_0, \varphi) \right]^{-1}. \quad (23)$$

It is the inverse of the second momentum of the Husimi function and can be considered as the participation ratio of $\bar{\rho}$ in the phase space. The definition of \mathcal{L} implies that it varies in the range $\mathcal{L} \in [0, N+1]$. For the extremely localized state, it is identical to a single point in phase space. This means $\mathcal{L} \simeq 1/(N+1)$ which vanishes as $N \rightarrow \infty$. However, for the state that uniformly covers the phase space, we have $Q(n_0, \varphi) = 1/(N+1)$, resulting in $\mathcal{L} = N+1$ in this case. Hence, the growth of the value of \mathcal{L} implies the increase of the degree of delocalization of $\bar{\rho}$ in phase space. In Fig. 6(e), we plot \mathcal{L} as a function of $\delta\xi$ for several system sizes with $\xi_i = 1$ which yields $\delta\xi_c = 0.5$ [cf. Eq. (14)]. Irrespective of the system size, the localization measure exhibits a peak in the vicinity of the critical point, indicating that the state $\bar{\rho}$ has the highest degree of delocalization near the critical point, as seen in Fig. 6(b). This further verifies that the DPT-I is a dynamical consequence of the separatrix in the underlying classical systems.

B. DPTs-II: cusps in survival probability

The second kind of DPTs, DPTs-II, are usually triggered by different physical origin than DPTs-I. Even though the connections between this two kinds of DPTs have been revealed in several systems from different aspects [12–15, 29, 32, 41, 42], such as the the links between the zeros in the order parameters of DPTs-I and the critical points of DPTs-II, a general understanding on the mechanism of DPTs-II remains unknown.

In the pioneering work [5], a DPT-II is defined as the onset of singularities in the evolution of the initial state survival probability rate function at critical times. For a given initial state $|\psi_0\rangle$, its survival probability and associated rate function are defined as

$$S_P(t) = |\langle \psi_0 | e^{-iH_f t} | \psi_0 \rangle|^2, \quad R(t) = -\frac{1}{N} \ln S_P(t), \quad (24)$$

where N denotes the system size. The definition of DPTs-II is based on the resemblance of the amplitude of $S_p(t)$ to the thermal partition function $\mathcal{Z}(\beta) = \text{Tr}e^{-\beta H}$. This can be seen by considering the amplitude of $S_P(t)$ as a complex function with variable $z = it$, so that $\mathcal{A}_P(z) = \langle \psi_0 | e^{-zH} | \psi_0 \rangle = \text{Tr}e^{-zH}$. Thus, one can extend the concept of equilibrium phase transition, which signifies as singularities in the free energy density $F = -(1/\beta N) \ln \mathcal{Z}(\beta)$, to DPTs-II by identifying the rate function $R(t)$ as the dynamical free energy density. Analogy to the thermal phase transition,

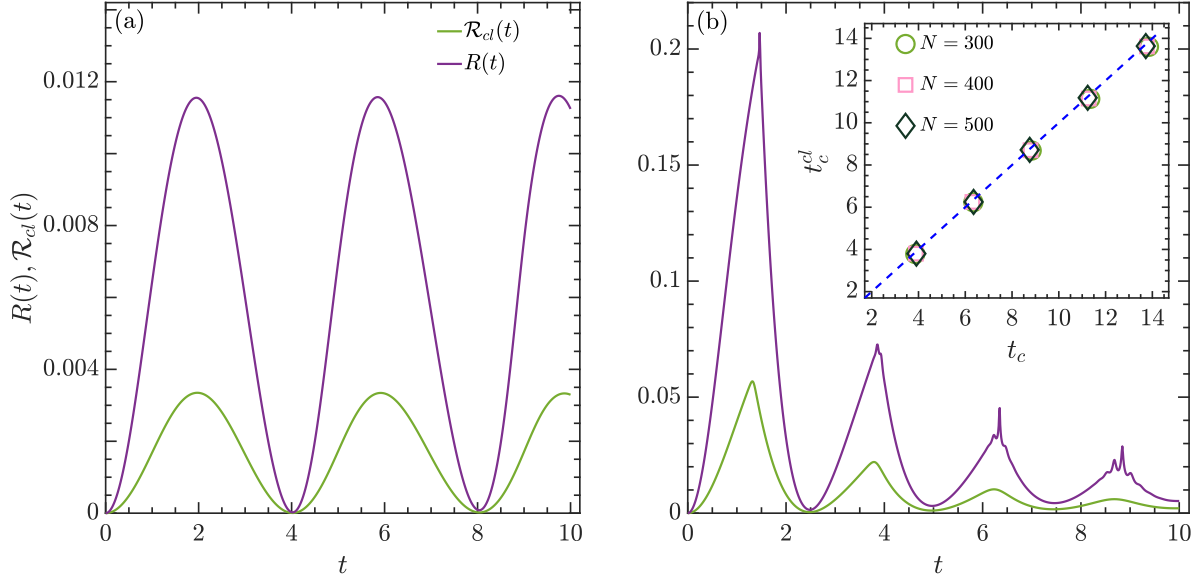


FIG. 10. Semiclassical rate function $\mathcal{R}_{cl}(t)$ in (26), along with quantum counterpart $R(t)$ in (24) for (a) $\delta\xi = 0.2$, (b) $\delta\xi = 1$. Inset in panel (b) plots the critical times t_c^{cl} corresponding to kinks in $\mathcal{R}_{cl}(t)$ and t_c obtained from the nonanalytical behavior in $R(t)$ for several system sizes. The blue dashed line denotes the linear fitting with the form $t_c^{cl} = t_c$. Other parameters: $N = 300$ and $\xi_i = 1$, so that $\delta\xi_c = 0.5$ [cf. Eq. (14)]. All quantities are dimensionless.

the occurrence of a DPT-II is captured by nonanalytical in $R(t)$ at certain times. Moreover, the correspondence of $\mathcal{A}_P(z)$ and $\mathcal{Z}(\beta)$ also motivates numerous investigations of the relationship between nonequilibrium and equilibrium phase transitions [5, 6, 16, 17, 37].

Previous works have been demonstrated that the presence of a DPT-II requires quench the control parameter across the ground state quantum phase transition [4, 5, 86]. However, the recent studies in the long-range interacting and collective systems were found that DPTs-II can be divided into two distinct scenarios [18, 33, 40]. The first one, on the one hand, is dubbed as regular dynamic phase, characterized by appearing of the first nonanalytical cusp always before the first minimal value of the rate function [40]. The critical quench that leads to the regular dynamical phase are independent of the ground state phase transition [2]. On the other hand, a DPT-II can also emerge even for the quenches that are not crossed the ground state quantum phase transition, resulting in the so called anomalous dynamical phase [18, 40]. In contrast to the regular dynamical phase, a main signature of the anomalous dynamical phase is the cusps occurring only after the first minimum of the rate function [33, 40]. The following of this subsection devotes to explore the DPT-II in spinor BEC from both quantum and semiclassical perspectives.

In Figs. 7(a)-7(c), we plot the evolution of $S_P(t)$ for different $\delta\xi$ values and several system sizes with $\xi_i = 1$, which results in $\delta\xi_c = 0.5$. If $\delta\xi < \delta\xi_c$, as seen in Fig. 7(a), $S_P(t)$ behaves as a simply smooth and periodic function of time and it always takes positive values during the evolution. However, $S_P(t)$ exhibits a completely different behavior when $\delta\xi > \delta\xi_c$, as exemplified in Fig. 7(c). Although it still shows a regular oscillation, the magnitude of $S_P(t)$ bears a time decay in this case. In particular, we see that $S_P(t)$ vanishes periodically with time. The vanish of $S_P(t)$ is also presented for the critical quench, but no periodic behavior can be observed in the evolution of $S_P(t)$, as illustrated in Fig. 7(b).

The observed features of $S_P(t)$ indicate the existence of DPT-II for the case of $\delta\xi \geq \delta\xi_c$. This is clearly visible in Figs. 7(d)-7(f), where we display the corresponded rate functions of $S_P(t)$ in Figs. 7(a)-7(c). The obvious kinks in $R(t)$ at certain critical times t_c in Figs. 7(e) and 7(f) are strikingly contrasted to the smooth behavior shown in Fig. 7(d) and unveil the occurrence of DPT-II in the system when $\delta\xi \gtrsim \delta\xi_c$. Moreover, due to the first nonanalytical point appears before the the first minimum of $R(t)$, the phase of DPT-II is regular. The presence of DPT-II for $\delta\xi \gtrsim \delta\xi_c$ is further revealed as the nonsmoothness in the time derivative of $R(t)$, as demonstrated in Figs. 7(g)-7(i), where we plot $dR(t)/dt$ as a function of time.

More insights on the properties of DPT-II can be gained by considering the evolution of the quantum state in the

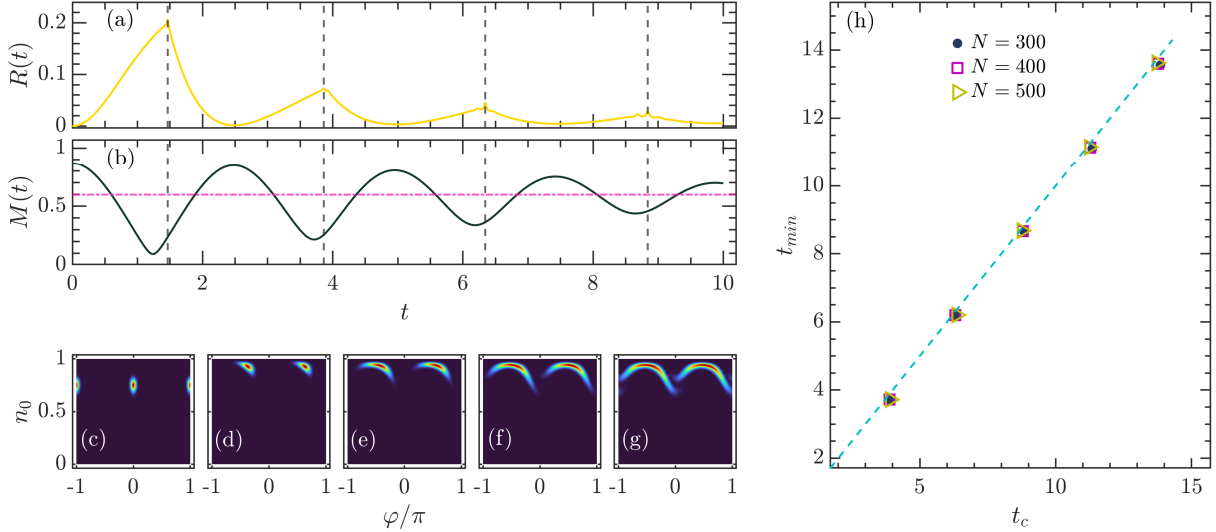


FIG. 11. (a) Rate function $R(t)$ and (b) the evolution of $M(t)$ for $\delta\xi = 1$ with $N = 300$ and $\xi_i = 1$. In this case, one can find the critical quench is given by $\delta\xi_c = 0.5$ [cf. Eq. (14)]. The vertical dashed lines in panels (a) and (b) signal the critical times of DPT-II, while the horizontal dot-dashed line in (b) marks the long time averaged value of $M(t)$, obtained from Eq. (17). (c)-(g): Snapshots of the Husimi function at (c) $t = 0$, (d) $t = t_{c,1} = 1.4632$, (e) $t = t_{c,2} = 3.860$, (f) $t = t_{c,3} = 6.345$, and (g) $t = t_{c,4} = 8.840$ for the same parameters as in panels (a) and (b). (h) Times t_{min} , associated with the local minimal of $M(t)$ and the critical times t_c of DPT-II for several system sizes with $\xi_i = 1$ and $\delta\xi = 1$. The dashed line represents the linear function of the form $t_{min} = t_c$. The axes in all figures are dimensionless.

classical phase space. To this end, let us focus on the Husimi function of the evolved state, calculated as

$$\mathcal{Q}_t(n_0, \varphi) = \langle \alpha | \rho_t | \alpha \rangle = \left| \sum_k e^{-iE_k^f t} \langle \alpha | E_k^f \rangle \langle E_k^f | \alpha \rangle \right|^2, \quad (25)$$

where ρ_t is the density of the evolved state given in Eq. (11). The evolution of $\mathcal{Q}_t(n_0, \varphi)$ at different times for several values of $\delta\xi$ has been plotted in Fig. 8 for a system with $N = 300$ and $\xi_i = 1$. In this case, we have $\delta\xi_c = 0.5$, according to Eq. (14). We clearly see that the specific evolution process of $\mathcal{Q}_t(n_0, \varphi)$ is determined by the strength of the quench. For small $\delta\xi$, since the quenched system without enough energy to overcome the saddle point, the evolution of $\mathcal{Q}_t(n_0, \varphi)$ is confined within two disjointed phase space regions and exhibits a periodically rotation around the initial state, as illustrated in the top row of Fig. 8. This leads to the regular oscillation behavior in survival probability with nonzero values. Hence, the rate $R(t)$ is a simply periodic and smooth function. This explains the absence of DPT-II when $\delta\xi < \delta\xi_c$. In contrast, as soon as $\delta\xi \gtrsim \delta\xi_c$, the quenched system acquires enough energy so that it enables to explore both regions freely, as observed in the middle and bottom rows of Fig. 8. This means the quenched state can exhibit a zero overlap with initial state at certain times, leading to zero values in the survival probability. As a consequence, the rate $R(t)$ behaves as a nonanalytical function with kinks at different critical times t_c for $\delta\xi \gtrsim \delta\xi_c$, and thus the onset of DPT-II. These results are more clearly visible in Fig. 9, where we plot the marginal distribution of $\mathcal{Q}_t(n_0, \varphi)$ at several time steps for different $\delta\xi$ values. The overlap between $\mathcal{Q}_{t \neq 0}(n_0)$ and $\mathcal{Q}_{t=0}(n_0)$ is alway finite for $\delta\xi < \delta\xi_c$, while it allows to take zero or very tiny value as long as $\delta\xi \gtrsim \delta\xi_c$.

To make aforementioned points strong, we study the semiclassical counterpart of the survival probability and associated rate function. By considering the normalization condition of the Husimi function, we define them as

$$\mathcal{S}_{cl}(t) = \frac{N+1}{2\pi} \int dn_0 d\varphi [\mathcal{Q}_t(n_0, \varphi) \mathcal{Q}_0(n_0, \varphi)]^{1/2}, \quad \mathcal{R}_{cl}(t) = -\frac{1}{N} \ln \mathcal{S}_{cl}(t). \quad (26)$$

Here, the definition of $\mathcal{S}_{cl}(t)$ guarantees $\mathcal{S}_{cl}(t) \leq 1, \forall t$, such as the quantum survival probability. The features observed in the evolution of $\mathcal{Q}_t(n_0, \varphi)$ and associated marginal distribution in Figs. 8 and 9 imply that $\mathcal{R}_{sc}(t)$ should be smooth function when $\delta\xi < \delta\xi_c$, whereas it would become nonanalytical with kinks at certain times for $\delta\xi > \delta\xi_c$ case. This is verified in Fig. 10, where $\mathcal{R}_{sc}(t)$ along with its quantum counterpart $R(t)$ for different $\delta\xi$ values are plotted. Irrespective of $\delta\xi$ value, the resemblance in the behaviors of $\mathcal{R}_{cl}(t)$ and $R(t)$ can be clearly seen. To quantitatively

confirm the equivalence between \mathcal{R}_{cl} and $R(t)$, we compare the critical times t_c^{cl} , associated with the kinks in $\mathcal{R}_{cl}(t)$ to the times t_c that are extracted from the nonanalytical points in the evolution of $R(t)$. In the inset of Fig. 10(b), we plot t_c^{cl} as a function of t_c for several system sizes. The dependence of t_c^{cl} on t_c is well captured by a linear function of the form $t_c^{cl} = t_c$, demonstrating the usefulness of the semiclassical approach in studying DPT-II. Moreover, the coincidence between t_c^{cl} and t_c further corroborates that the presence of DPT-II can also be attributed to the existence of the separatrix in the corresponding classical dynamics.

As the separatrix in the classical system links to both DPT-I and DPT-II, it is natural to ask what is the relationship between them. Although the previous studies in the long-range interacting spin models have shown that the presence of DPT-II is associated with the vanish of the order parameter of DPT-I [13, 18, 29, 40, 41], a general connection between two kinds of DPTs remains an open question. Here, at the end of this section, let us address this question in spin-1 BEC system by investigating whether the nonanalytical times in $R(t)$ are linked to the times when the evolution of the order parameter $M(t)$ of DPT-I takes local minima. In Fig. 11(a), we plot $R(t)$ for $\xi_i = 1$ and $\delta\xi = 1$ with $N = 300$, and Fig. 11(b) shows the evolution of $M(t)$ for same parameters. One can see that the nonanalytical points in $R(t)$, i. e., critical times t_c , are close to the times t_{min} , at which $M(t)$ present local minima. One can expect the observed deviations between t_c and t_{min} can be suppressed by increasing system size. Moreover, the Husimi functions for initial time and each critical time t_c are also depicted in Figs. 11(c)-11(f). As we can see, the overlap of the evolved Husimi function with the initial one is zero or very tiny at the critical times t_c of DPT-II. Meanwhile, the Husimi function at each critical time t_c is highly condensed around $n_0 = 1$, resulting in the local minima in $M(t)$. These features of the Husimi function explains why the critical times of DPT-II are correlated with the local minima of $M(t)$. To make such connection more clearer, we compare the critical times t_c to the local minima times t_{min} of $M(t)$ in Fig. 11(h). We see that t_{min} exhibits an obvious linear dependence on t_c and it converges to the critical times with increasing system size. Hence, the local minima in $M(t)$ indeed reveals the presence of DPT-II.

IV. CONCLUSIONS

In this work, a detailed investigation of the DPTs in a many body quantum system, namely the celebrated spin-1 BEC, has been performed. As the spin-1 BEC can be controlled in a highly precision and has rich phases, it can be used as a suitable platform to investigate the DPTs. We have shown that two types of DPTs are presented as the control parameter has been quenched through the critical value. A semiclassical analysis results in an analytical expression of the critical quench and reveals that both types of DPTs can be recognized as the dynamical consequence of the separatrix in the underlying classical dynamics.

The characterizations of two types of DPTs have been scrutinized by various quantum and semiclassical properties. Specifically, we uncover the signatures of DPT-I by analyzing the time evolution of the order parameter, $M(t)$, and its long time average features for both quantum and semiclassical systems. Semiclassically, depending on the quenching strength, the semiclassical dynamics is either locked within two disconnected regions in the phase space, or explore the whole phase space. This leads to a dramatic change in the quantum dynamics of the order parameter. We have shown that the quantum dynamics follows the semiclassical counterpart up to a certain time for the quenches that below the critical value. However, the agreement between quantum and semiclassical dynamics disappears quickly when the quench strength larger than the critical value. Both quantum and semiclassical dynamics exhibit particular behaviors at the critical quench. The presence of DPT-I is more clearly revealed by the first dip of $M(t)$. We have shown that the first dip of $M(t)$ behaves as an order parameter of DPT-I. It has nonzero value if the quench strength below the critical value, while it becomes zero in the semiclassical limit once the quench strength above the critical value. By performing a scaling analysis, we have confirmed that the first dip of $M(t)$ is indeed an appropriate order parameter of DPT-I for our system. We have also examined the properties of the long time averaged order parameter, \bar{M} , and demonstrated that the dependence of \bar{M} on the quenching strength is well captured by the diagonal ensemble. In contrast to the case of the first dip in $M(t)$, DPT-I appears as a sudden dip in the behavior of \bar{M} . By employing the Husimi function, we have shown that the presence of the dip in \bar{M} around the critical point is due to the extension of the evolved state over the separatrix.

Regarding to DPT-II, we have shown that it can only happen when the quenching strength above the critical value, while it disappears as long as the quenching strength smaller than the critical value. The occurrence of DPT-II is signified by the kinks in the rate function of the initial state survival probability at different critical times. A semiclassical explanation of the emergence of DPT-II has been discussed by means of Husimi function. We have found that the onset of DPT-II depends on whether the quenched system has enough energy to straddle the saddle point freely. For quenching strengths that below the critical value, the quenched system does not have sufficient energy to surpass the saddle point. As a result, the evolution of the system is confined within the initial position, leading to a nonzero overlap between the evolved and initial states and the absence of DPT-II. On the contrary, as soon as the quench strength above the critical value, the quenched system acquires enough energy so that it can pass through

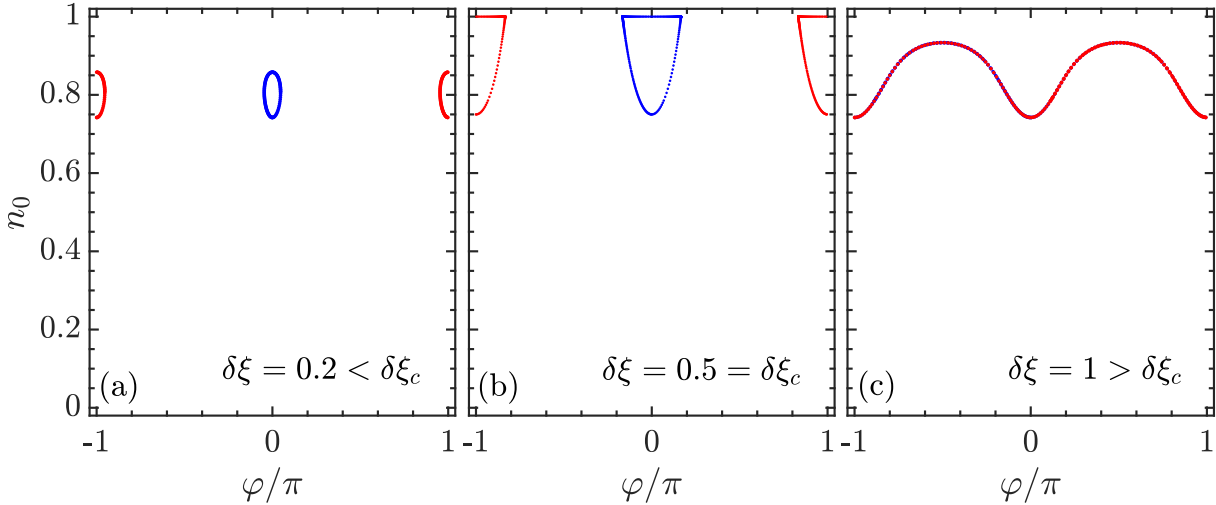


FIG. 12. Snapshots of the semiclassical dynamics of the spin-1 BEC for several $\delta\xi$ values, obtained from the classical equations of motion (6) in the main text. Here, the system is evolved up to $t = 22$ with initial condition $(\cos\varphi_i, n_{0,i}) = [\pm 1, (2 + \xi_i)/4]$. The dynamics of the initial condition $\cos\varphi_i = 1$ is plotted by blue dots, while red dots correspond to the case of $\cos\varphi_i = -1$. Other parameter: $\xi_i = 1$, so that $\delta\xi_c = 0.5$ [cf. Eq. (14)]. The axes in all figures are dimensionless.

the saddle point. This means that the evolved state will exhibit a zero overlap with the initial state at certain times. Thus, the rate function undergoes a nonanalytical behavior at different times, indicating the presence of DPT-II. The correctness of this semiclassical picture of DPT-II is further verified by the agreement between the behaviors of the quantum and semiclassical rate functions. We can therefore conclude that both DPTs-I and DPTs-II in the spin-1 BEC are triggered by the separatrix in the corresponding classical system. This conclusion is further evidenced by the direct link between the critical times of DPT-II and the times at which $M(t)$ presents local minima. A numerical calculation has been suggested that these two times are consistent with each other in the semiclassical limit.

A continuation of this work is to analyze the scaling properties of DPTs-II. The classification of DPTs-II remains an open question, despite it is valuable for understanding DPTs-II [97–99]. It would also be interesting to extend our present analysis for ferromagnetic condensate to the antiferromagnetic case, which undergoes a first order ground state quantum phase transition as the control parameter passes through the critical value. The DPTs-I in the antiferromagnetic spinor condensate has been studied in recent works [59, 60], but the studies of DPTs-II is still lacking. Moreover, it is worth stressing that our work verifies the usefulness of the semiclassical approach in comprehending DPTs. Hence, we hope that the present work can motivate other semiclassical studies of DPTs in many body quantum systems that have the well-defined semiclassical limit. As a final remark, owing to the spin-1 BEC is a highly controllable platform and the emergence of various advanced techniques that enable to measure the density matrices, we expect that our findings could stimulate more experimental researches on the properties of DPTs.

ACKNOWLEDGMENTS

This work was supported by the National Science Foundation of China under Grant No. 11805165; the Zhejiang Provincial Nature Science Foundation under Grant Nos. LQ22A040006 and LY20A050001. Q. W. acknowledges support from the Slovenia Research and Innovation Agency (ARIS) under the Grant Nos. J1-4387 and P1-0306.

Appendix A: Semiclassical dynamics of the spin-1 BEC

To get a better understanding of the semiclassical origins of DPTs and provide further evidence of quantum-classical correspondence of nonequilibrium dynamics, we consider the semiclassical dynamics in this appendix.

In the semiclassical limit $N \rightarrow \infty$, the equations of motion of the spin-1 BEC is given by Eq. (6) in the main text. The semiclassical dynamics is obtained by solving those equations with the initial condition is given by the ground state of the system, that is, $(\cos\varphi_i, n_{0,i}) = [\pm 1, (2 + \xi_i)/4]$. The resulting semiclassical dynamics in the phase space for different quenching strengths are plotted in Fig. 12. Here, we have $\xi_i = 1$, so that $\delta\xi_c = 0.5$. As illustrated

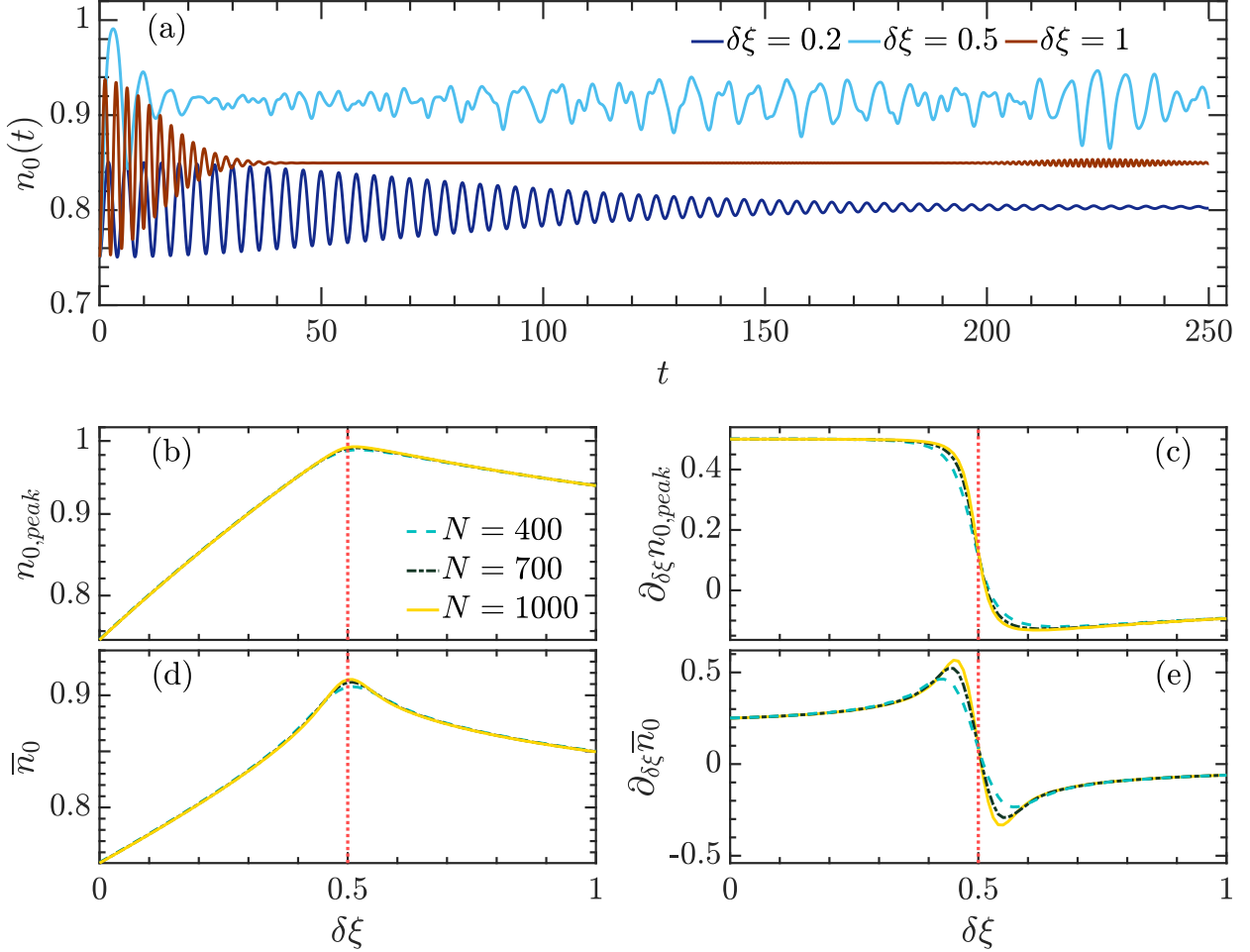


FIG. 13. (a) Time evolution of $n_0(t)$ for several values of $\delta\xi$ with $N = 1000$. (b) First peak of $n_0(t)$, denoted by $n_{0,peak}$, and (c) its derivative with respect to $\delta\xi$, denoted by $\partial_{\delta\xi} n_{0,peak}$, as a function of $\delta\xi$ for different system sizes [see the legend in panel (b)]. (d)-(e) Long time average of $n_0(t)$, \bar{n}_0 , and $\partial_{\delta\xi} \bar{n}_0$ as a function of $\delta\xi$ for the same system sizes as in panels (b) and (c). Here, \bar{n}_0 is obtained by averaging $n_0(t)$ in the time interval $t \in [0, 1000]$. Other parameter: $\xi_i = 1$. Vertical red dotted lines in panels (b)-(e) denote $\delta\xi_c = 0.5$, obtained from Eq. (14). The axes in all figures are dimensionless.

in Fig. 12(b), the semiclassical dynamics shows an obvious separatrix at the critical quench strength. For quenches that below the critical value, the system does not have enough energy to surpass the saddle point, leading to the semiclassical dynamics is locked within two disconnected regions, as seen in Fig. 12(a). On the contrary, once $\delta\xi > \delta\xi_c$, the system has sufficient energy to move freely between both regions. As a consequence, two disjointed regions merge together and the semiclassical dynamics can visit the whole phase space, as shown in Fig. 12(c). It is worth pointing out that the semiclassical dynamics constitutes the skeleton of the time evolution of Husimi function in phase space, as illustrated in Fig. 8.

Appendix B: Dynamics of the density of spin-0 component

Further characterizations of DPTs can be revealed by exploring the dynamics of the density of spin-0 component, defined as

$$n_0 = \frac{a_0^\dagger a_0}{N}. \quad (B1)$$

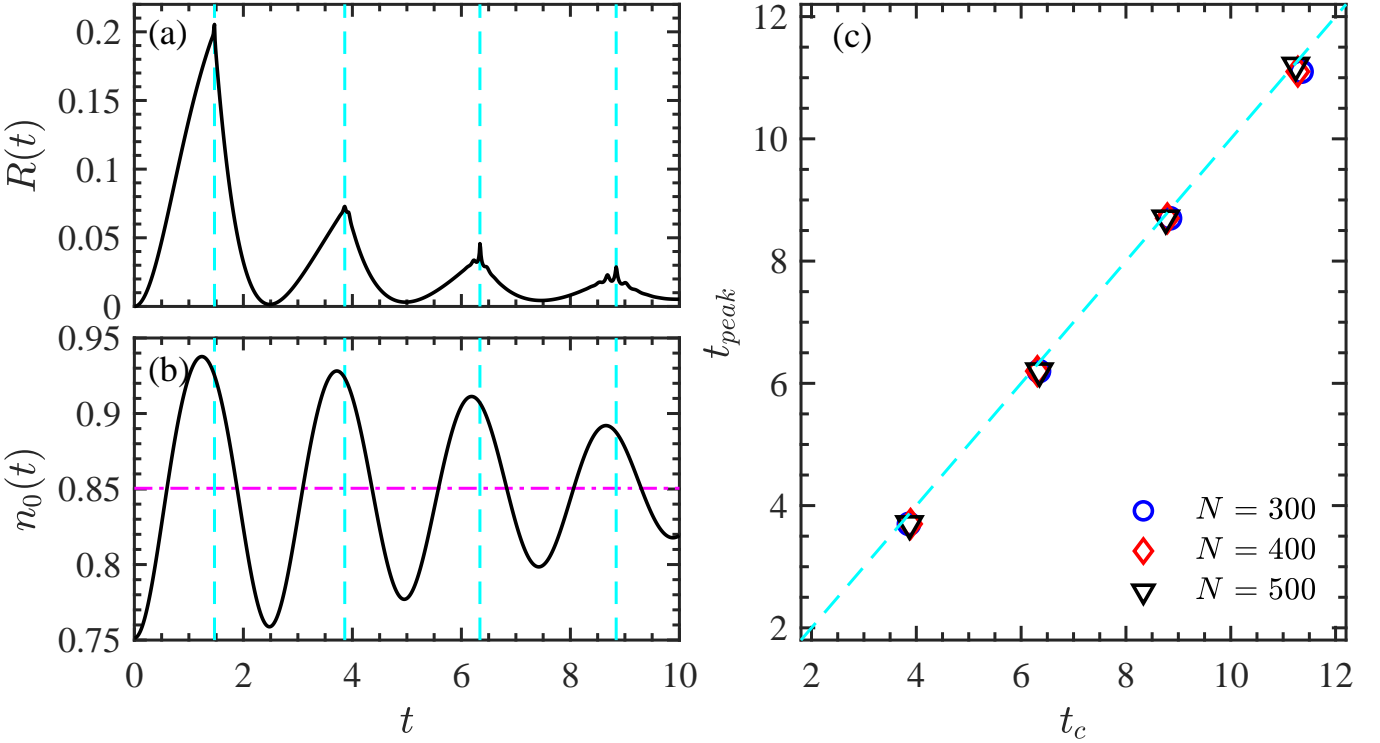


FIG. 14. (a) Rate function $R(t)$ and (b) the time evolution $n_0(t)$ for $\delta\xi = 1$ with system size $N = 300$. Vertical dashed lines in panels (a) and (b) mark the critical times of DPT-II, while the horizontal dot-dashed line in panel (b) denotes the value of \bar{n}_0 in (B4). (c) Times t_{peak} , defined as the instants when the local peak in $n_0(t)$ present, and the critical times t_c of DPT-II for different system sizes N with $\delta\xi = 1$. The dashed line corresponds to the function $t_{peak} = t_c$. Other parameter: $\xi_i = 1$, associated with $\delta\xi_c = 0.5$ [cf. Eq. (14)]. The axes in all figures are dimensionless.

As a conventional detectable quantity in spinor BECs, n_0 has been employed to experimentally probe the DPT-I in antiferromagnetic spin-1 BEC [28, 59]. Here, we use it to scrutinize the signatures of two types of DPTs in ferromagnetic spin-1 BECs.

After the quench, the evolution of n_0 is given by

$$n_0(t) = \text{Tr}[\rho(t)n_0] = \sum_{k,m} e^{i(E_k^f - E_m^f)} c_k^* c_m n_{0,km}, \quad (\text{B2})$$

where $n_{0,km} = \langle E_k^f | n_0 | E_m^f \rangle$ and $c_s = \langle E_s^f | \psi_0 \rangle$ with $s = m, k$. The time evolution of $n_0(t)$ for several quenching strengths with $N = 1000$ and $\xi_i = 1$ is plotted in Fig. 13(a). One can see that the evolution of $n_0(t)$ shows a remarkable change as the value of $\delta\xi$ passes through the critical value of DPT-I, which gives by $\delta\xi_c = 0.5$ for $\xi_i = 1$ case, such as we have observed in the dynamics of $M(t)$. For both $\delta < \delta\xi_c$ and $\delta\xi > \delta\xi_c$ cases, $n_0(t)$ exhibits a regular behavior, while it irregularly oscillates around a saturation value with small amplitude for the critical quenching strength.

The above observed behaviors of $n_0(t)$ lead us to explore the signatures of DPT-I in the short and long time evolutions of $n_0(t)$. For the short time case, we focus on the first peak of $n_0(t)$, defined as $n_{0,peak} = n_0(t = t_{peak})$ with t_{peak} being the time when the first peak present. The results shown in Fig. 13(a) indicate that $n_{0,peak}$ should have a maximal value at $\delta\xi_c$. This is indeed what we see in Fig. 13(b), where we plot $n_{0,peak}$ as a function of $\delta\xi$ for different system sizes. The presence of DPT-I at $\delta\xi = \delta\xi_c$ can be more clearly revealed by the behavior of the derivative of $n_{0,peak}$ with respect to $\delta\xi$. In Fig. 13(c), we plot $\partial_{\delta\xi} n_{0,peak} = \partial n_{0,peak} / \partial(\delta\xi)$ as a function of $\delta\xi$ for the same system sizes as in Fig. 13(b). We see that $\partial_{\delta\xi} n_{0,peak}$ undergoes an obvious jump from 0.5 to a negative value near $\delta\xi_c$, regardless of the system size N . However, the sharpness of the jump increases with increasing N . Thus, the jump in $\partial_{\delta\xi} n_{0,peak}$ acts as a precursor of DPT-I in a finite system. It is worth pointing out that $\partial_{\delta\xi} n_{0,peak}$ curves for different system sizes cross at $\delta\xi = 0.5$, which is in consistence with the critical point of DPT-I [cf. Eq. (14)].

To see how the occurrence of DPT-I gets reflected in the long time dynamics of $n_0(t)$, we consider the long time

average of $n_0(t)$, defined as

$$\bar{n}_0 = \lim_{T \rightarrow \infty} \frac{1}{T} \int_0^T dt n_0(t). \quad (\text{B3})$$

Inserting $n_0(t)$ in (B2) into above equation and employing the fact that $E_k \neq E_m$ for $k \neq m$, one find that \bar{n}_0 can be simplified to

$$\bar{n}_0 = \sum_k |c_k|^2 n_{0,kk}. \quad (\text{B4})$$

Figure 13(d) illustrates how the \bar{n}_0 depends on $\delta\xi$ for different system sizes. Clearly, the underlying DPT-I results in a peak in the behavior of \bar{n}_0 , suggesting \bar{n}_0 can be used as a probe of DPT-I. The ability of \bar{n}_0 to detect DPT-I is further verified by investigating its derivative with respect to $\delta\xi$. In Fig. 13(e), we demonstrate how the $\partial_{\delta\xi}\bar{n}_0$ varies as a function of $\delta\xi$ for several system sizes. The dramatic change in the behavior of $\partial_{\delta\xi}\bar{n}_0$ is clearly visible near the critical quenching strength. In particular, the variation of $\partial_{\delta\xi}\bar{n}_0$ with $\delta\xi$ for different N also cross at $\delta\xi = 0.5$, indicating the presence of DPT-I in the thermodynamic limit. This is in agreement with the analytical result given by Eq. (14).

Let us finally discuss the relationship between the dynamics of n_0 and the second kind of DPTs. To this end, we plot the rate function $R(t)$ and $n_0(t)$ in Figs. 14(a) and 14(b), respectively, for $\delta\xi = 1$ and $N = 300$ with $\xi_i = 1$. One can clearly see that the critical times t_c of DPT-II are associated with the instants of time t_{peak} , corresponding to the location of peaks in $n_0(t)$. Although the finite system size leads to an obvious deviation between t_c and t_{peak} , the agreement between them should be enhanced by increasing N . We compare the local peak times t_{peak} of $n_0(t)$ to the critical times t_c for different system sizes in Fig. 14(c). As shown in the figure, the variation of t_{peak} with t_c is well captured by a linear function, which converges to the form $t_{peak} = t_c$ with increasing N . Hence, the local peak in $n_0(t)$ behaves as a witness of DPT-II.

[1] M. Eckstein and M. Kollar, *Phys. Rev. Lett.* **100**, 120404 (2008).
[2] B. Sciolla and G. Biroli, *J. Stat. Mech.* **2011**, P11003 (2011).
[3] J. Marino, M. Eckstein, M. S. Foster, and A. M. Rey, *Rep. Prog. Phys.* **85**, 116001 (2022).
[4] M. Heyl, A. Polkovnikov, and S. Kehrein, *Phys. Rev. Lett.* **110**, 135704 (2013).
[5] M. Heyl, *Rep. Prog. Phys.* **81**, 054001 (2018).
[6] A. A. Zvyagin, *Low Temp. Phys.* **42**, 971 (2016).
[7] M. Moeckel and S. Kehrein, *Phys. Rev. Lett.* **100**, 175702 (2008).
[8] M. Eckstein, M. Kollar, and P. Werner, *Phys. Rev. Lett.* **103**, 056403 (2009).
[9] B. Sciolla and G. Biroli, *Phys. Rev. Lett.* **105**, 220401 (2010).
[10] R. J. Lewis-Swan, S. R. Muleady, D. Barberena, J. J. Bollinger, and A. M. Rey, *Phys. Rev. Res.* **3**, L022020 (2021).
[11] R. Puebla, *Phys. Rev. B* **102**, 220302 (2020).
[12] B. Žunkovič, A. Silva, and M. Fabrizio, *Philos. Trans. R. Soc. A* **374**, 20150160 (2016).
[13] B. Žunkovič, M. Heyl, M. Knap, and A. Silva, *Phys. Rev. Lett.* **120**, 130601 (2018).
[14] A. Sehrawat, C. Srivastava, and U. Sen, *Phys. Rev. B* **104**, 085105 (2021).
[15] T. Hashizume, I. P. McCulloch, and J. C. Halimeh, *Phys. Rev. Res.* **4**, 013250 (2022).
[16] C. Karrasch and D. Schuricht, *Phys. Rev. B* **87**, 195104 (2013).
[17] M. Schmitt and S. Kehrein, *Phys. Rev. B* **92**, 075114 (2015).
[18] J. C. Halimeh and V. Zauner-Stauber, *Phys. Rev. B* **96**, 134427 (2017).
[19] U. Bhattacharya and A. Dutta, *Phys. Rev. B* **96**, 014302 (2017).
[20] R. Jafari, H. Johannesson, A. Langari, and M. A. Martin-Delgado, *Phys. Rev. B* **99**, 054302 (2019).
[21] U. Mishra, R. Jafari, and A. Akbari, *J. Phys. A: Math. Theor.* **53**, 375301 (2020).
[22] R. Jafari and A. Akbari, *Phys. Rev. A* **103**, 012204 (2021).
[23] R. Jafari, A. Akbari, U. Mishra, and H. Johannesson, *Phys. Rev. B* **105**, 094311 (2022).
[24] P. Jurcevic, H. Shen, P. Hauke, C. Maier, T. Brydges, C. Hempel, B. P. Lanyon, M. Heyl, R. Blatt, and C. F. Roos, *Phys. Rev. Lett.* **119**, 080501 (2017).
[25] J. Zhang, G. Pagano, P. W. Hess, A. Kyprianidis, P. Becker, H. Kaplan, A. V. Gorshkov, Z. X. Gong, and C. Monroe, *Nature* **551**, 601 (2017).
[26] S. Smale, P. He, B. A. Olsen, K. G. Jackson, H. Sharum, S. Trotzky, J. Marino, A. M. Rey, and J. H. Thywissen, *Science Advances* **5**, eaax1568 (2019).
[27] J. A. Muniz, D. Barberena, R. J. Lewis-Swan, D. J. Young, J. R. K. Cline, A. M. Rey, and J. K. Thompson, *Nature* **580**, 602 (2020).
[28] T. Tian, H.-X. Yang, L.-Y. Qiu, H.-Y. Liang, Y.-B. Yang, Y. Xu, and L.-M. Duan, *Phys. Rev. Lett.* **124**, 043001 (2020).
[29] J. Lang, B. Frank, and J. C. Halimeh, *Phys. Rev. B* **97**, 174401 (2018).

[30] A. Gambassi and P. Calabrese, *Europhys. Lett.* **95**, 66007 (2011).

[31] J. C. Halimeh, V. Zauner-Stauber, I. P. McCulloch, I. de Vega, U. Schollwöck, and M. Kastner, *Phys. Rev. B* **95**, 024302 (2017).

[32] A. Lerose, B. Žunkovič, J. Marino, A. Gambassi, and A. Silva, *Phys. Rev. B* **99**, 045128 (2019).

[33] A. L. Corps and A. Relaño, *Phys. Rev. B* **106**, 024311 (2022).

[34] A. L. Corps and A. Relaño, *Phys. Rev. Lett.* **130**, 100402 (2023).

[35] A. L. Corps, P. Pérez-Fernández, and A. Relaño, (2023), arXiv:2305.04643 [quant-ph].

[36] R. Jafari, *Sci. Rep.* **9**, 2871 (2019).

[37] S. Vajna and B. Dóra, *Phys. Rev. B* **89**, 161105 (2014).

[38] E. Canovi, P. Werner, and M. Eckstein, *Phys. Rev. Lett.* **113**, 265702 (2014).

[39] F. Andraschko and J. Sirker, *Phys. Rev. B* **89**, 125120 (2014).

[40] I. Homrighausen, N. O. Abeling, V. Zauner-Stauber, and J. C. Halimeh, *Phys. Rev. B* **96**, 104436 (2017).

[41] S. A. Weidinger, M. Heyl, A. Silva, and M. Knap, *Phys. Rev. B* **96**, 134313 (2017).

[42] J. Lang, B. Frank, and J. C. Halimeh, *Phys. Rev. Lett.* **121**, 130603 (2018).

[43] Ángel L. Corps and A. Relaño, “General theory for discrete symmetry-breaking equilibrium states,” (2023), arXiv:2303.18020 [quant-ph].

[44] Y. Kawaguchi and M. Ueda, *Phys. Rep.* **520**, 253 (2012).

[45] D. M. Stamper-Kurn and M. Ueda, *Rev. Mod. Phys.* **85**, 1191 (2013).

[46] B. Damski and W. H. Zurek, *Phys. Rev. Lett.* **99**, 130402 (2007).

[47] A. Lamacraft, *Phys. Rev. Lett.* **98**, 160404 (2007).

[48] M. Anquez, B. A. Robbins, H. M. Bharath, M. Boguslawski, T. M. Hoang, and M. S. Chapman, *Phys. Rev. Lett.* **116**, 155301 (2016).

[49] M. Xue, S. Yin, and L. You, *Phys. Rev. A* **98**, 013619 (2018).

[50] E. M. Bookjans, A. Vinit, and C. Raman, *Phys. Rev. Lett.* **107**, 195306 (2011).

[51] J. H. Kim, S. W. Seo, and Y. Shin, *Phys. Rev. Lett.* **119**, 185302 (2017).

[52] M. Prüfer, P. Kunkel, H. Strobel, S. Lannig, D. Linnemann, C.-M. Schmied, J. Berges, T. Gasenzer, and M. K. Oberthaler, *Nature* **563**, 217 (2018).

[53] Z. Chen, T. Tang, J. Austin, Z. Shaw, L. Zhao, and Y. Liu, *Phys. Rev. Lett.* **123**, 113002 (2019).

[54] L.-Y. Qiu, H.-Y. Liang, Y.-B. Yang, H.-X. Yang, T. Tian, Y. Xu, and L.-M. Duan, *Science Advances* **6**, eaba7292 (2020).

[55] L. E. Sadler, J. M. Higbie, S. R. Leslie, M. Vengalattore, and D. M. Stamper-Kurn, *Nature* **443**, 312 (2006).

[56] J.-y. Choi, W. J. Kwon, and Y.-i. Shin, *Phys. Rev. Lett.* **108**, 035301 (2012).

[57] S. Kang, S. W. Seo, H. Takeuchi, and Y. Shin, *Phys. Rev. Lett.* **122**, 095301 (2019).

[58] L. Zhou, J. Kong, Z. Lan, and W. Zhang, *Phys. Rev. Res.* **5**, 013087 (2023).

[59] H.-X. Yang, T. Tian, Y.-B. Yang, L.-Y. Qiu, H.-Y. Liang, A.-J. Chu, C. B. Dağ, Y. Xu, Y. Liu, and L.-M. Duan, *Phys. Rev. A* **100**, 013622 (2019).

[60] Y. Huang, Y. Ding, J. Xu, J. Liu, H. Wang, and H.-N. Xiong, *Phys. Rev. A* **106**, 022430 (2022).

[61] M.-S. Chang, C. D. Hamley, M. D. Barrett, J. A. Sauer, K. M. Fortier, W. Zhang, L. You, and M. S. Chapman, *Phys. Rev. Lett.* **92**, 140403 (2004).

[62] D. M. Stamper-Kurn, M. R. Andrews, A. P. Chikkatur, S. Inouye, H.-J. Miesner, J. Stenger, and W. Ketterle, *Phys. Rev. Lett.* **80**, 2027 (1998).

[63] S. Yi, O. E. Müstecaplıoğlu, C. P. Sun, and L. You, *Phys. Rev. A* **66**, 011601 (2002).

[64] M. Gabrielli, L. Pezzè, and A. Smerzi, *Phys. Rev. Lett.* **115**, 163002 (2015).

[65] C. K. Law, H. Pu, and N. P. Bigelow, *Phys. Rev. Lett.* **81**, 5257 (1998).

[66] J. Jie, Q. Guan, and D. Blume, *Phys. Rev. A* **100**, 043606 (2019).

[67] F. Gerbier, A. Widera, S. Fölling, O. Mandel, and I. Bloch, *Phys. Rev. A* **73**, 041602 (2006).

[68] C. D. Hamley, C. S. Gerving, T. M. Hoang, E. M. Bookjans, and M. S. Chapman, *Nat. Phys.* **8**, 305 (2012).

[69] Z. Zhang and L.-M. Duan, *Phys. Rev. Lett.* **111**, 180401 (2013).

[70] P. Feldmann, M. Gessner, M. Gabrielli, C. Klemp, L. Santos, L. Pezzè, and A. Smerzi, *Phys. Rev. A* **97**, 032339 (2018).

[71] P. Feldmann, C. Klemp, A. Smerzi, L. Santos, and M. Gessner, *Phys. Rev. Lett.* **126**, 230602 (2021).

[72] Z.-X. Niu and Q. Wang, *Phys. Rev. A* **107**, 033307 (2023).

[73] B. Meyer-Hoppe, F. Anders, P. Feldmann, L. Santos, and C. Klemp, “Excited-state phase diagram of a ferromagnetic quantum gas,” (2023), arXiv:2301.10655 [cond-mat.quant-gas].

[74] P. Cejnar, P. Stránský, M. Macek, and M. Kloc, *J. Phys. A: Math. Theor.* **54**, 133001 (2021).

[75] M. Caprio, P. Cejnar, and F. Iachello, *Ann. Phys.* **323**, 1106 (2008).

[76] P. Stránský, M. Macek, and P. Cejnar, *Ann. Phys.* **345**, 73 (2014).

[77] W. Zhang, D. L. Zhou, M.-S. Chang, M. S. Chapman, and L. You, *Phys. Rev. A* **72**, 013602 (2005).

[78] M. Rautenberg and M. Gärtnner, *Phys. Rev. A* **101**, 053604 (2020).

[79] Y. Qiao and F. Grossmann, *Phys. Rev. A* **103**, 042209 (2021).

[80] T. M. Hoang, H. M. Bharath, M. J. Boguslawski, M. Anquez, B. A. Robbins, and M. S. Chapman, *Proc. Natl. Acad. Sci. USA* **113**, 9475 (2016).

[81] M. Gutzwiller, *Chaos in Classical and Quantum Mechanics*, Interdisciplinary Applied Mathematics (Springer New York, 2013).

[82] P. Ribeiro, J. Vidal, and R. Mosseri, *Phys. Rev. E* **78**, 021106 (2008).

- [83] B. Sciolla and G. Biroli, *Phys. Rev. B* **88**, 201110 (2013).
- [84] M. Gring, M. Kuhnert, T. Langen, T. Kitagawa, B. Rauer, M. Schreitl, I. Mazets, D. A. Smith, E. Demler, and J. Schmiedmayer, *Science* **337**, 1318 (2012).
- [85] T. Mori, T. N. Ikeda, E. Kaminishi, and M. Ueda, *J. Phys. B: At. Mol. Opt. Phys.* **51**, 112001 (2018).
- [86] M. Heyl, *Phys. Rev. Lett.* **113**, 205701 (2014).
- [87] S. De Nicola, A. A. Michailidis, and M. Serbyn, *Phys. Rev. Lett.* **126**, 040602 (2021).
- [88] A. L. Corps, P. Stránský, and P. Cejnar, *Phys. Rev. B* **107**, 094307 (2023).
- [89] G. J. Milburn, J. Corney, E. M. Wright, and D. F. Walls, *Phys. Rev. A* **55**, 4318 (1997).
- [90] H. Veksler and S. Fishman, *New J. Phys.* **17**, 053030 (2015).
- [91] M. Srednicki, *J. Phys. A: Math. Gen.* **32**, 1163 (1999).
- [92] L. D'Alessio, Y. Kafri, A. Polkovnikov, and M. Rigol, *Adv. Phys.* **65**, 239 (2016).
- [93] K. Husimi, *Proc. Phys. Math. Soc. Jpn* **22**, 264 (1940).
- [94] E. Wigner, *Phys. Rev.* **40**, 749 (1932).
- [95] A. Altland and F. Haake, *Phys. Rev. Lett.* **108**, 073601 (2012).
- [96] A. Altland and F. Haake, *New J. Phys.* **14**, 073011 (2012).
- [97] M. Heyl, *Phys. Rev. Lett.* **115**, 140602 (2015).
- [98] S. Bandyopadhyay, A. Polkovnikov, and A. Dutta, *Phys. Rev. Lett.* **126**, 200602 (2021).
- [99] R. V. Bhat and S. Bera, “Distinguishing dynamical quantum criticality through local fidelity distances,” (2023), [arXiv:2308.00435 \[cond-mat.stat-mech\]](https://arxiv.org/abs/2308.00435).